AD-A210 549

SECU

MENTATION PAGE

Form Approved
OMB No. 0704-0188

1a. F UNCLASSIFIED	1b. RESTRICTIVE MARKINGS

2a. SECURITY CLASSIFICATION AUTHORITY	3. DISTRIBUTION / AVAILABILITY OF REPORT
2b. DECLASSIFICATION / DOWNGRADING SCHEDULE	Approved for public release; distribution is unlimited.

4. PERFORMING ORGANIZATION REPORT NUMBER(S)	5. MONITORING ORGANIZATION REPORT NUMBER(S)
	AFOSR-TR- 89-0993

6a. NAME OF PERFORMING ORGANIZATION	6b. OFFICE SYMBOL (If applicable)	7a. NAME OF MONITORING ORGANIZATION
Univ of California		AFOSR/NP

6c. ADDRESS (City, State, and ZIP Code)	7b. ADDRESS (City, State, and ZIP Code)
Dept of Elect. Eng & Comp. Sci. La Jolla, CA 92093	Building 410, Bolling AFB DC 20332-6448

8a. NAME OF FUNDING / SPONSORING ORGANIZATION	8b. OFFICE SYMBOL (If applicable)	9. PROCUREMENT INSTRUMENT IDENTIFICATION NUMBER
AFOSR	NP	AFOSR-87-0351

8c. ADDRESS (City, State, and ZIP Code)	10. SOURCE OF FUNDING NUMBERS			
Building 410, Bolling AFB DC 20332-6448	PROGRAM ELEMENT NO. 61102F	PROJECT NO. 2301	TASK NO. A7	WORK UNIT ACCESSION NO.

11. TITLE (Include Security Classification)
(U) STUDIES OF HIGH POWER DENSITY, PICO-SECOND RISE-TIME LIGHT ACTIVATED SEMICONDUCTOR SWITCH

12. PERSONAL AUTHOR(S)
Paul L. Yu

13a. TYPE OF REPORT	13b. TIME COVERED	14. DATE OF REPORT (Year, Month, Day)	15. PAGE COUNT
Final	FROM 9/1/87 TO 12/31/88		106

16. SUPPLEMENTARY NOTATION

17.	COSATI CODES		18. SUBJECT TERMS (Continue on reverse if necessary and identify by block number)
FIELD	GROUP	SUB-GROUP	Carrier Dynamics, Diode, Electrical Power Switching, Optical Excitations, Photodiodes
	20.12		
	10.01		

19. ABSTRACT (Continue on reverse if necessary and identify by block number)

See Other Side

DTIC
ELECTE
JUL 19 1989
S B D

20. DISTRIBUTION / AVAILABILITY OF ABSTRACT	21. ABSTRACT SECURITY CLASSIFICATION
☐ UNCLASSIFIED/UNLIMITED ☐ SAME AS RPT ☐ DTIC USERS	UNCLASSIFIED
22a. NAME OF RESPONSIBLE INDIVIDUAL Bruce L. Smith, Lt Col, USAF	22b. TELEPHONE (Include Area Code) (202) 767-4906	22c. OFFICE SYMBOL AFOSR/NP

DD Form 1473, JUN 86   Previous editions are obsolete.

SECURITY CLASSIFICATION OF THIS PAGE
UNCLASSIFIED

19. ABSTRACT (cont)

The carrier dynamics of the diode which is related to its electrical power switching behaviors is investigated in this program. A model is developed where the carrier transport and Maxwell equations are incorporated and self-consistent electrical field profiles, current density and carrier profiles are obtained in the PIN diode. Both low and high level optical excitations as well as low and high applied bias situations can be described by this model. The transient behavior of the diode switch at different optical energy levels is now well understood, while conventional theory for photodiodes at low level excitation and at low bias cannot be applied to cases for high level excitation and high bias. As a circuit element, the rise time of the switch under these circumstances depends on the time the internal field is cancelled out by mobile carriers generated. The predicted input energy dependence and the transmission line impedance dependence of the rise time compare well with experimental results. The model also suggests the experimental configuration for obtaining power in the GW range. Finally, a preliminary investigation is made on the effects of avalanche multiplication on the performance of the diode switch.

Final Report on

Studies of High Power Density, Picosecond Rise-Time

Light Activated Semiconductor Switch

P.K.L.Yu

University of California at San Diego

Department of Electrical and Computer Engineering

Mail Code: R-007

UCSD La Jolla, CA 92093

Tel: (619)-534-6180

Abstract

The carrier dynamics of the diode which is related to its electrical power switching behaviors is investigated in this program. A model is developed where the carrier transport and Maxwell equations are incorporated and self-consistent electrical field profiles, current density and carrier profiles are obtained in the PIN diode. Both low and high level optical excitations as well as low and high applied bias situations can be described by this model. The transient behavior of the diode switch at different optical energy levels is now well understood, while conventional theory for photodiodes at low level excitation and at low bias cannot be applied to cases for high level excitation and high bias. As a circuit element, the rise time of the switch under these circumstances depends on the time the internal field is cancelled out by mobile carriers generated. The predicted input energy dependence and the transmission line impedance dependence of the rise time compare well with experimental results. The model also suggests the experimental configuration for obtaining power in the GW range. Finally, a preliminary investigation is made on the effects of avalanche multiplication on the performance of the diode switch.

I. Introduction

In the last program, the light activated semiconductor switches made of silicon junction diode have been demonstrated. A novel optical delay line has been designed in sampling the laser pulses to these switches. Electrical power switched by this device of 6.7 MW has been reported[1]. Subsequent experiments performed at Energy Compression Research Corporation have demonstrated power far exceeding this value. However, the rise time of the electrical pulses remains in the 100 ps range. Also, the photo-quantum efficiency of the device was not independently measured, therefore the overall efficiency of the device is only roughly estimated.

The goals of this present program are to investigate physical mechanisms responsible for the rise time limitation of this device and to study designs to achieve higher electrical power and current density from these switches. Three mechanisms have been suggested to explain the rise time observed: the transmission line impedance mismatch at the diode; the lateral current diffusion; and the collapse of the electric field in the junction upon carrier generation.

Both the transmission line effect and the lateral current diffusion have been investigated in details in the beginning of the present program and they are found to be in the picosecond and sub-picosecond second and thus are too small to account for the observed rise time of the device.

In an effort to understand the rise time behavior, we have looked closely into the device dynamics in conjunction with an external circuit. Also, there has been a strong interest in developing a complete theoretical analysis of the device which can account for other observed behaviors of the device effects. The following sections describe the model and the computer simulation built on this model. The results obtained, as described in section V, have been compared to experiment (section VI) and they are in good agreement. This allows us to design further experiment based on this model.

Among the graduate research assistants participated, Mr. Vincent D. Lew has finished his M. Sc. thesis (see Appendix 1) under this program and Mr. C. K. Sun will include in his Ph. D. thesis the following model which he principally developed under this program. A paper summarizing this work will soon be submitted to journal for publication.

II. Master Equations

The switching characteristics of the device studied in this program are basically governed by the carrier dynamics inside the depletion region of the diode. They are also affected by the nature of the metal-semiconductor interface region. For low and medium electric field, the Boltzmann's transport equation is sufficient and is employed throughout this work. As mentioned, to analyze the carrier dynamics, an accurate computer simulation program has been developed under this program where three sets of equations are solved self-consistently inside the device including the bulk p and n regions, the depletion region and the the contact regions. These are the current density equations, continuity equations and Maxwell equations and are described as follows:

2.1. Current Density Equations:

Current density equations describe the carrier transport under the influence of the electric field and diffusion:

$$J_n = q \mu_n \, nE + q \, D_n \, \nabla n \tag{1}$$

$$J_p = q \mu_p \, pE - q \, D_p \, \nabla p \tag{2}$$

where μ's and D's are the mobilities and diffusion coefficients for electrons and holes. Since the electric field inside the junction area may vary over a large range, the mobility cannot be taken to be constant. Instead, a field dependent mobility is used and is given as[2]:

$$\mu = \frac{\mu_o}{\left[1 + \left[\frac{E}{E_c} \right]^y \right]^{1/y}} \cdot \tag{3}$$

where values of μ_o, E_c and y for electrons and holes in silicon are listed in Table I. The diffusion coefficients are related to the mobilities through the Einstein relation:

$$D_p = \mu_p \, \frac{kT}{q} \tag{4}$$

$$D_n = \mu_n \, \frac{kT}{q} \tag{5}$$

	μ_o (cm^2/V.s)	E_c (Volt/cm)	y
electron	1350	8,000	2
hole	480	20,000	1

TABLE 1

2.2. Continuity Equations:

Continuity equations are basically statements of charge conservation. They describe the net amount of carrier concentration as a function of time at any point taken into account carrier generations, recombinations and transport. These equations can be stated as follows:

$$\frac{\partial n}{\partial t} = G_n - U_n + \frac{1}{q} \nabla \cdot J_n \tag{6a}$$

$$\frac{\partial p}{\partial t} = G_p - U_p - \frac{1}{q} \nabla \cdot J_p \tag{6b}$$

where G_n and G_p are the respective electron and hole generation rate, U_n and U_p are the recombination rate of electron and hole. In our work, the generation is from the laser irradiation and avalanche multiplication. Both are functions of time and position within the device. The carrier generation resulted from avalanche processes depends on the ionization potential for electrons (α) and holes (β) both of which are field dependent quantities. For the case of silicon, the following expression are used in the simulation[3]:

$$\alpha = \frac{E}{3.6 \times \exp \left[\dfrac{-1.95 \times 10^6}{E \left(1 + \dfrac{E}{1.07 \times 10^5} \right)} + 1.36 \times 10^4 \right]} \tag{7a}$$

$$\beta = \frac{E}{5.0 \times \exp \left[\dfrac{-3.1 \times 10^6}{E \left(1 + \dfrac{E}{1.11 \times 10^5} \right)} + 1.55 \times 10^4 \right]} \tag{7b}$$

where the electric field E is measured in units of V/cm. Since the recombination time in silicon

is in the microsecond and millisecond range and the time interval of interest for the transient behavior of the switch is in the picosecond and nanosecond range, the recombination process is ignored in our model.

2.3. Maxwell Equations:

Maxwell equations are used to determine the electric field inside the junction for a given carrier distribution and the total current output to an external loading circuit. Here only two of the four equations are used.

$$\nabla \times H = \varepsilon \frac{\partial E}{\partial t} + J_n + J_p = J_{total} \tag{8}$$

$$\nabla \cdot E = \frac{\rho}{\varepsilon} \tag{9}$$

where Eq. (8) calculates the total current density and Eq. (9) is the Poisson equation commonly used for solving the electric field within the device. It turns out that Eqs. (8) and (9) are equivalent in principle. Starting with the divergence of Eq (8), one obtains,

$$\nabla \cdot \nabla \times H = \nabla \cdot J_{total} = \nabla \cdot \left[J_n + J_p + \varepsilon \frac{\partial E}{\partial t} \right] = 0 \tag{10}$$

From Eqs. (6), assuming $G_n = G_p$ and $U_n = U_p$, and together with Eq. (10) one gets

$$\varepsilon \frac{\partial}{\partial t}(\nabla \cdot E) + q \left[\frac{\partial}{\partial t} (n-p) \right] = 0$$

or

$$\frac{\partial}{\partial t} \left[\nabla \cdot E + \frac{q}{\varepsilon} (n-p) \right] = 0$$

This implies $\nabla \cdot E + \frac{q}{\varepsilon} (n-p)$ is a constant and is related to the doping $\frac{q}{\varepsilon} \left[N_d^+ - N_a^- \right]$. Thus, we have $\nabla \cdot E = \frac{q}{\varepsilon} \left[p-n + N_d^+ - N_a^- \right]$, which is Equation (9).

Therefore, only one equation is needed to solve for the electric field. Eq (8) is chosen instead of the Poisson equation because the effect of the load impedance on the current was not included explicitly in Eqs. (6) and (9). This may lead to charge divergence in the simulation programs. On the other hand, with Eq. (9), the electric field can be solved as follows:

$$J_n + J_p + \varepsilon \frac{\partial E}{\partial t} = J_{total} = \frac{V_d - V_{n-p}}{AR} \tag{11}$$

where V_d is the biasing voltage to the diode, V_{n-p} is the voltage drop across the diode, "A" is the surface area of the diode and R is the equivalent load impedance of the circuit. V_{n-p} is obtained by integrating the electric field over the length of the device. Eq. (11) thus provide a self consistent way to calculate the the total current taken into account the voltage drop on the diode. In the final simulation, the electric field and the J_{total} obtained self consistently from equation (11) are found to be more accurate than those obtained from equation (9). This is largely due to the fact that the computational error accumulated in the displacement current term can be huge even when the electric field is off just a little bit because the time increment "dt" can be very small. This uncertainty in the displacement current give rise to to instability in the value of J_{total} along the depletion region.

III. Boundary Condition

The exact nature of the semiconductor-metal contact is still a mystery at present. For most cases, the continuity of the electric field and current across the ohmic contact region is assumed. In general, contact properties between metal and semiconductor can be modeled as:

$$V_B = F(J_B) \tag{12}$$

where V_B is the voltage drop across the contact, J_B is the current density flow through it and F is some function related to the carrier transparent parameters at the contact region. For our case, ideal ohmic contact behaviors are assumed, thus V_B equals zero and

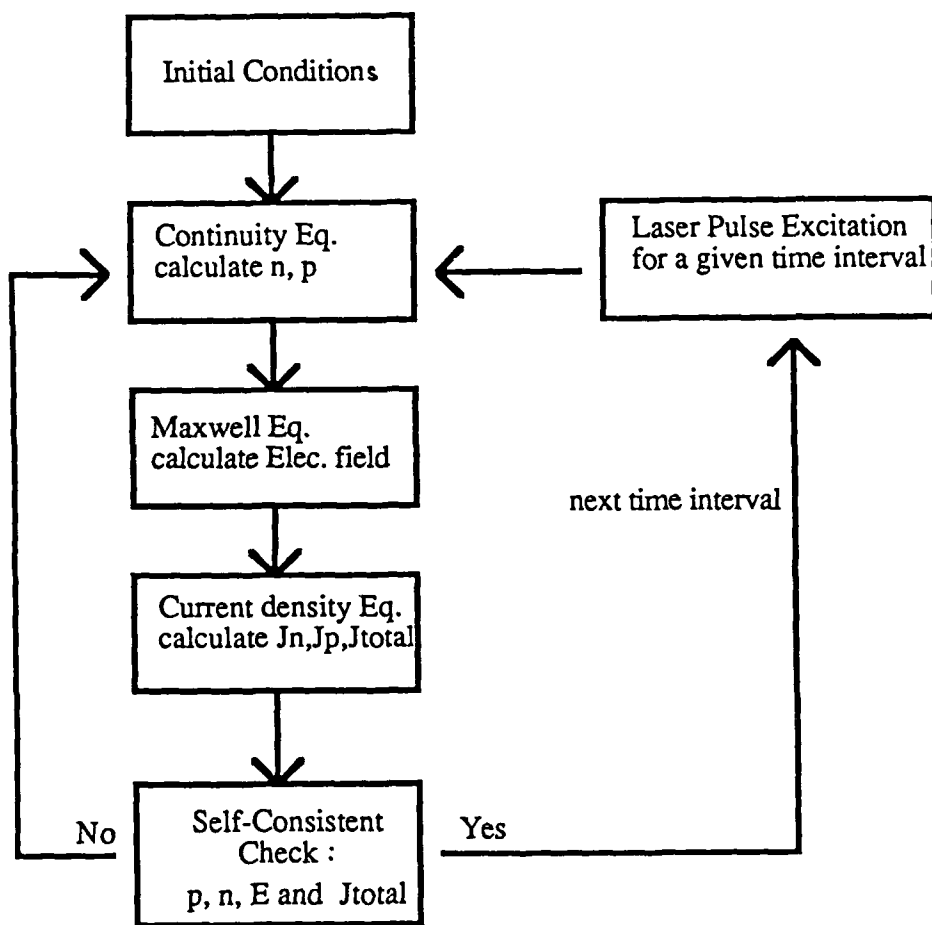$$J_n = 0 \quad \text{(for p-side contact)} \tag{13}$$

Figure 1   Block diagram representation of the
            simulation program.

$$J_p = 0 \quad \text{(for n–side contact)} \tag{14}$$

Eqs (13) ar $\cdot$ (14) exclude the injection of minority carriers from the contact to the bulk regions. In the simulation program, Eq. (12) is involved in the calculation of V_{n-p}; Eqs. (13) and (14) are employed in Eqs. (6) and (7) for solving the carrier concentration close to contact regions.

IV. Computer Simulation Program

In section II, three sets of equations are introduced in analyzing the switching characteristics of the diode. Due to the field dependent mobility, the partial differential equations are essentially nonlinear and can only be solved numerically. To this end, we have developed a simulation program based on the finite difference method (see appendix 2). Figure 1 shows a block diagram representation of this program. In each time interval, there will a spatial distribution of electron-hole pairs generated by the laser excitation. The equivalent finite difference form of the continuity equation is then used to calculate the net carrier concentration at each point taken into account both carrier generation and transport. At this point the electric field is based on values obtained from the previous time interval. However, since both the carrier concentration and the electric field distribution are interrelated and are thus dynamic variables, an iterative loop is employed in each time interval until the carrier concentration and electric field reach self-consistent and steady state values. The constraint is that the total current remains constant throughout the device in the same interval, as has been implicitly stated in Eq. (11). The same procedure takes place when the program advances to the next time interval.

Several assumptions have been made in this program:

1. Since a planar diode structure is used in the actual experiment, it is reasonable to analyze the device dynamics in the one dimension.

2. The absorption depth for silicon material is about 0.08 cm, for convenience, the electron-hole pairs are assumed to be uniformly generated in the width dimension of the diode.
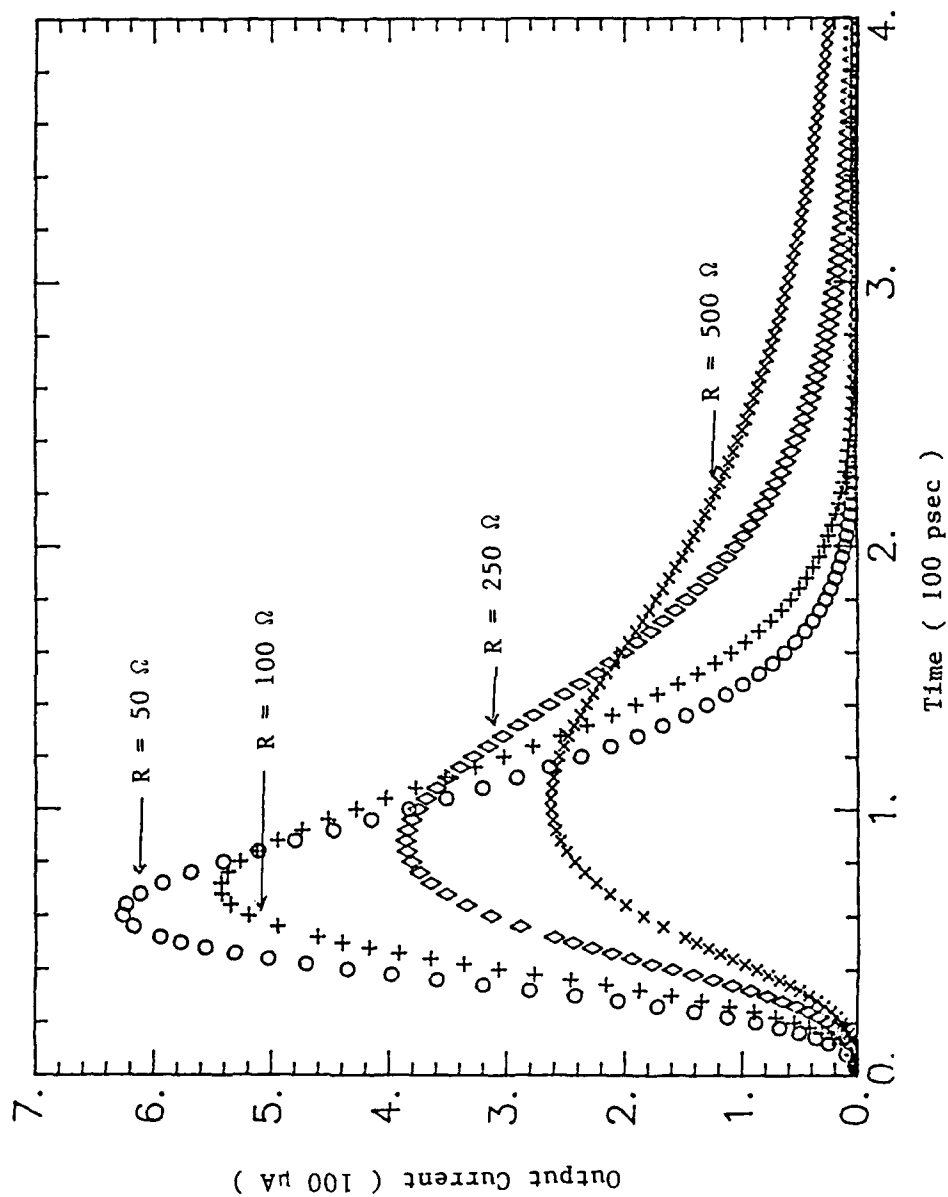
Figure 2   Simulated output response of silicon PIN photodiodes at low
optical excitation.

3. The recombination time constant for silicon material is in the milli-second range, and the time interval of interest is in the nanosecond and sun-nanosecond range, thus the recombination term in Eqs. (6) and (7) can be neglected.

4. For simplicity, the photo-quantum efficiency of the diode switch is assumed to be 100%.

V. Simulation Results

5.1. Comparison with the PIN photodiode case

In order to test the validity and accuracy of the simulation program developed, a comparison is made between the programming results and the experimentally observed photodiode behaviors reported in the literature[4-5]. The input to the program closely matches the dimension of a PIN photodiode where the p, intrinsic, and n regions are assumed to be 0.1 μms, 10 μm, and 0.1 μm respectively with corresponding background doping concentration takes value of $10^{18}cm^{-3}, 10^{13}cm^{-3}, 10^{17}cm^{-3}$. The area of the diode is $10^{-4}cm^2$, and the applied bias is 100 V. As in the usual operation of PIN photodiodes, a short duration, low energy optical pulse is incident on the diode. In our case, the quantum efficiency of the photodiode is assumed to be 100 %; the laser pulse is chosen to be 30 psec FWHM and the pulse energy is 0.6 nJ. The photodiode is taken to be in series with an output load whose impedance ranges from 50 Ω to 500 Ω in magnitude. The depletion capacitance of the diode calculated from the above data is around 0.1 pF. For this diode, the simulated current as a function time for different load impedance is depicted in Figure 2. It is noted that for the 50 Ω output load, the rise time is found to be 32 psec which is a combination of transit-time (5 psec), the laser pulse rise time (30 psec) and RC time constant (10 psec). In contrast, for the 500 Ω load case, the simulated rise time is about 100 psec which is dominated mainly by the RC time constant (100 psec).

The area beneath each curve in Fig. 2 equals the total amount of charges flowing in the external load as a result of absorption. The simulated response is found to be self-consistent
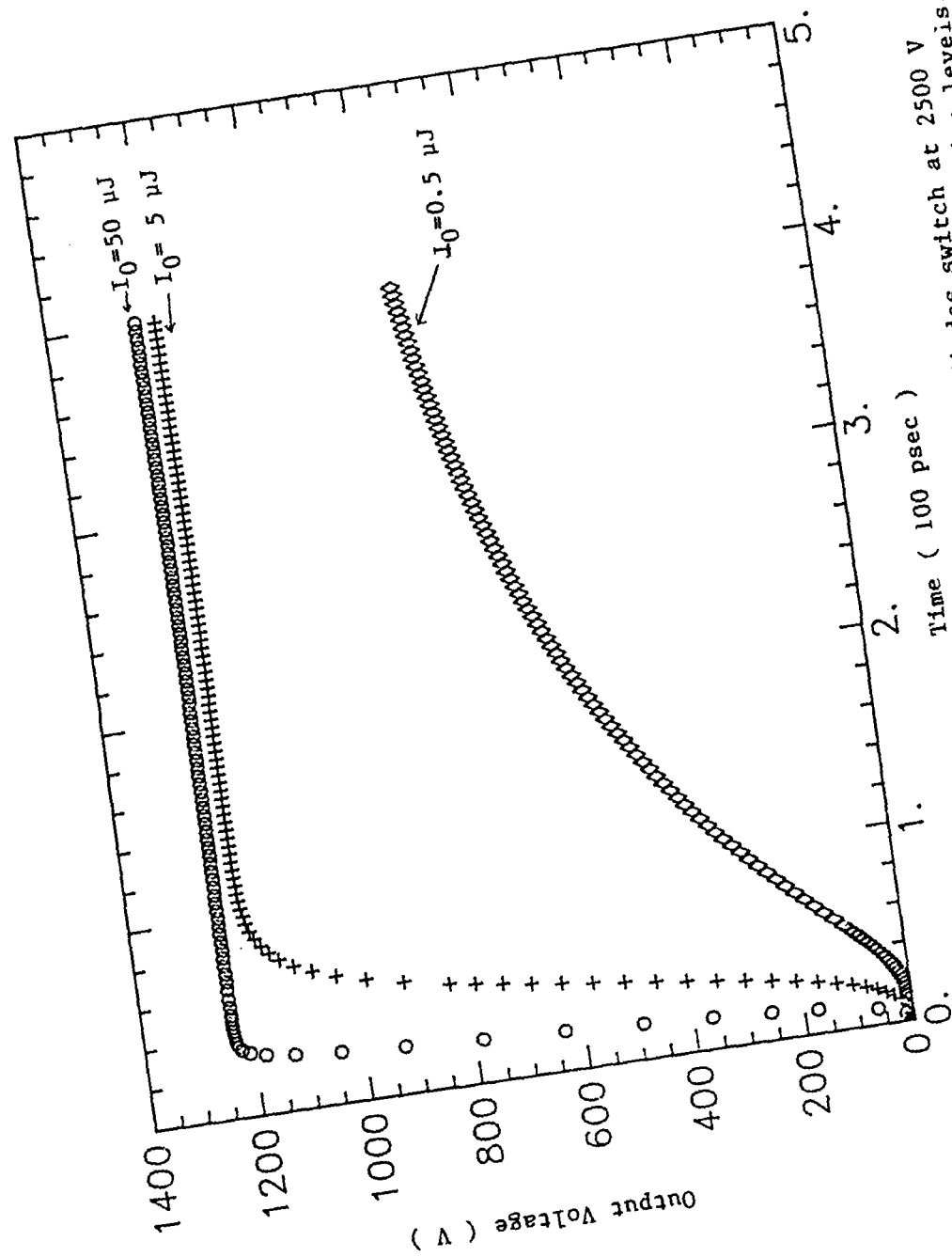
Figure 3   Simulated output response of the diodes switch at 2500 V
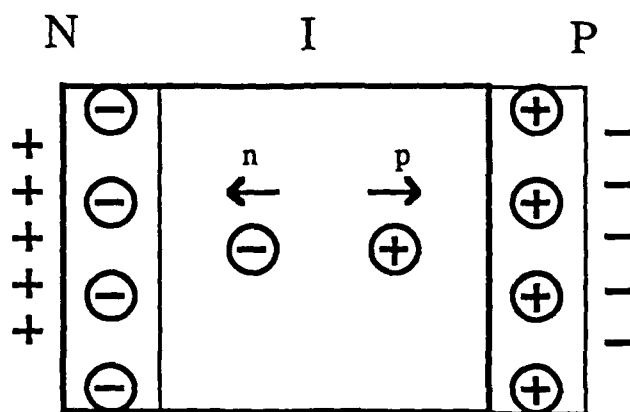applied voltage and at different optical excitation levels.

Figure 4   Schematic diagram of a PIN diode
            showing the separation of the
            changes inside the intrinsic region
            and their accumulation near the contact
            region.

with the initial laser input energy and the assumed quantum efficiency. The rise times are also in good agreement with experimental results reported in the literature.

5.2. Transient behaviors of the switch at high optical energy.

The next step is to investigate the transient behavior of the diode switch at high optical energy. The PIN diode studied in this case has a doping concentration of $10^{12} cm^{-3}$ in the intrinsic region, $10^{18} cm^{-3}$ in the P$^+$ region and $10^{17} cm^{-3}$ in the N region. The surface area of the diode is 0.5 cm^2, the intrinsic region width is 1600 μm. All these input data to the program correspond closely to the experimental conditions described in Section VI.

Figure 3 shows the simulated response as the laser pulse energy varies from 0.5 μJ to 50 μJ, with an applied voltage of 2500 V and an external load of 50 Ω. A decrease in the rise time, from more than 400 psec to less than 20 psec, is observed as the laser energy increases. It should be noted that the transit time for this diode is 16 nsec. On the other hand, the diode has a depletion capacitance of 0.3 pF, the RC time constant is 1.5 ps and is thus small when compared to the transit time.

Ordinarily, when subjected to an optical pulse whose energy is in the pJ range, the diode switch would respond like a photodiode with a rise time close to 4 nsec. However, according to the simulated results shown in Figure 3, the rise time shortens as the laser pulse energy increases. This phenomenon can be attributed to the collapse of the internal electric field as follows. The photogenerated electron-hole pairs are drifted apart by the biased electric field. When the number of these pairs are huge, the electric field created by the separation becomes sizable. Figure 4 is a schematic picture to illustrate the PIN diode response at high optical excitation. The separation of electrons and holes in the intrinsic region leaves behind charges which can be represented as net charges at both junction surfaces. These charges cancel the electric field from the ionized background dopants. As a result, most of the applied voltage falls on the external load and the output voltage (or current) reach a maximum value. This implies that the faster is the collapse of the electric field, the shorter is the rise time which can be much

n | i | p

(a)

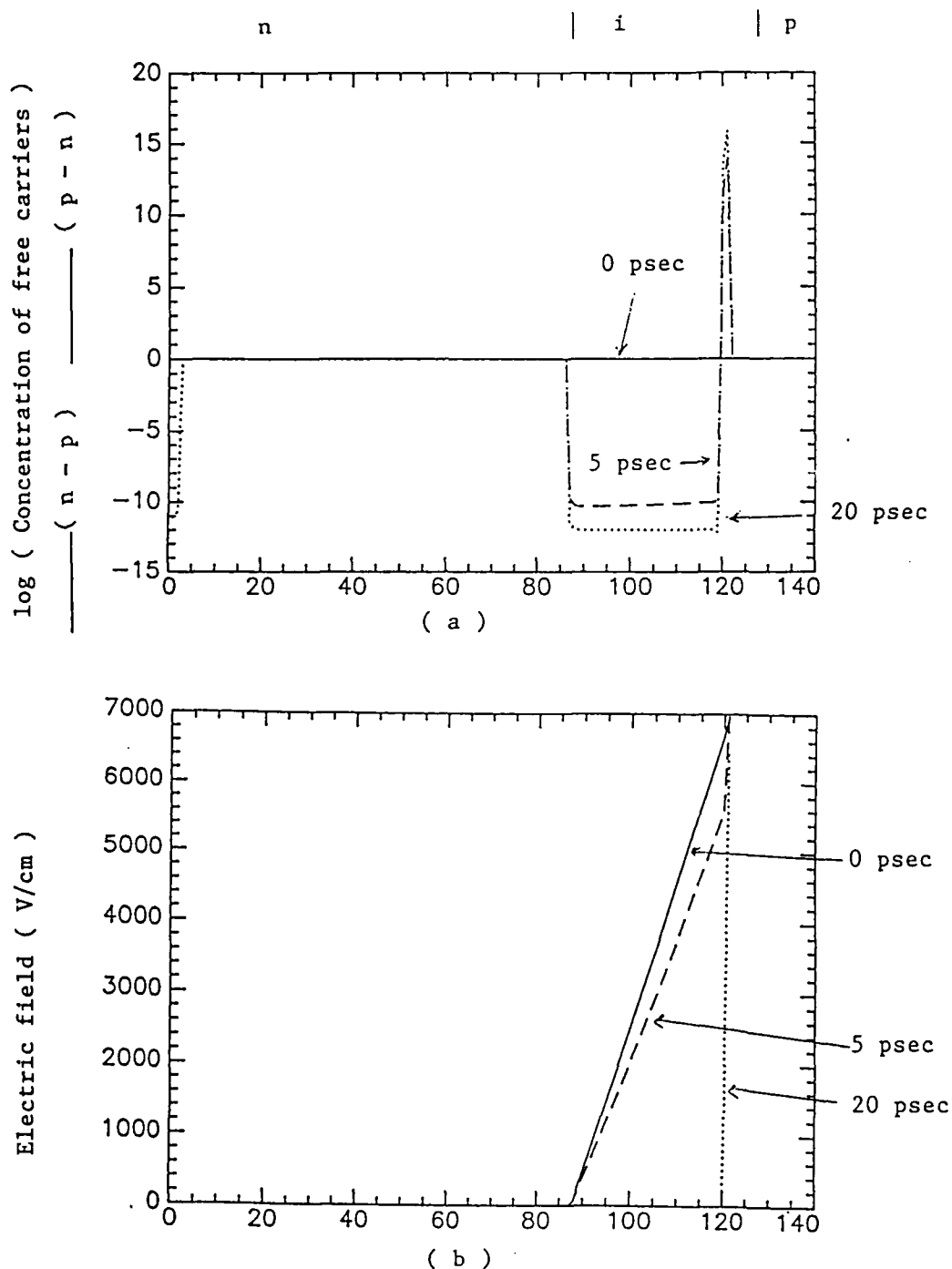(b)

Figure 5   Snapshots at different times of the
            (a) Net carriers concentration profiles
            (b) Electric field profile, the horizontal
                 scale (distance along the PIN diodes)
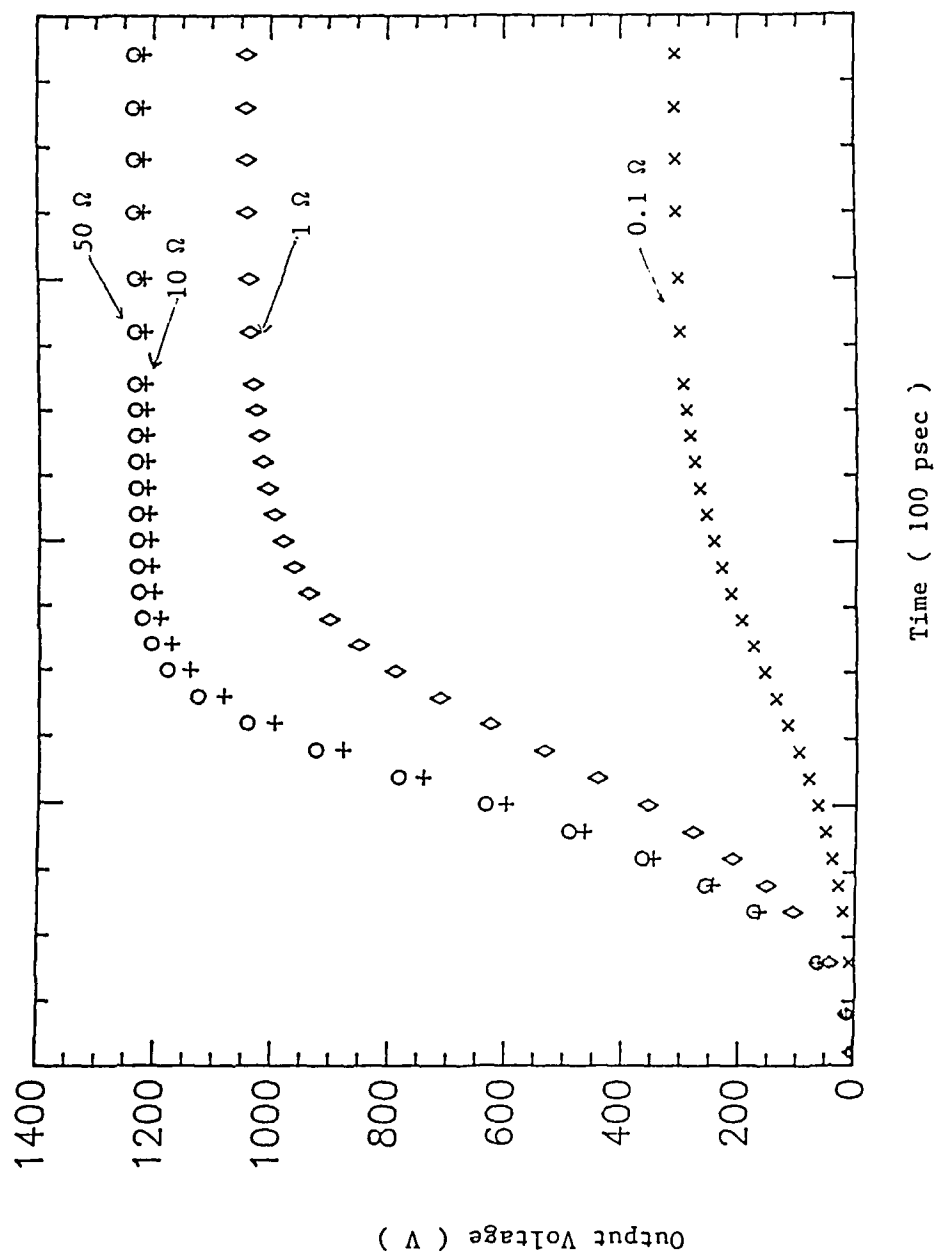   in units of 14 μm.

Figure 6   Simulated rise time of the same diode in Fig. 3 at different
load impedance. The input optical energy is held at 50 µJ.

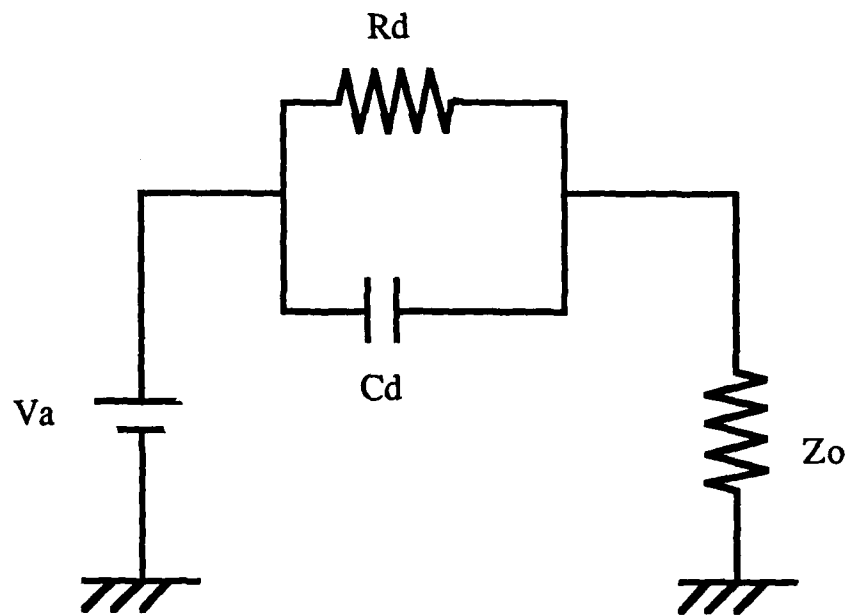Figure 7   Equivalent circuit model of the diode
            switch. R_d is the dynamic resistance,
            C_d is the diode depletion region capacitance.
            Z_0 is the load impedance.

shorter than the transit time. In contrast, for low level optical excitation, the effect of the photo-generated carrier on the internal electric field is small, then the transit time and the RC time constant determine the redistribution of the bias voltage. This agrees well with the simulated results shown in Figure 2, where the time corresponds to the peak current also corresponds to a minimum of the internal electric field inside the diode.

Several time-sequenced snapshots of the simulated electron and hole concentration profiles and the electric field profile are shown in Figures 5a and b respectively. In this case, the simulation was carried out for a diode with the same carrier profile and intrinsic region width as that in Figure 3, except the surface area is chosen to be 0.13 cm^2 and the applied voltage is 160 volts, which corresponds to another set of experimental condition.

5.3. Transient behaviors of the switch at various load impedance.

Of particular interest to generation of high power electrical pulses is behaviors of diode switches on transmission lines with different characteristic impedance. The simulated output responses of the diode switch at different load impedances (from 0.1 to 50 Ω) are shown in Figure 6. The input information to the program are the same as those used in Figure 3, the input optical energy is 50 μJ. The results shown in Figure 6 predict that the rise time decreases as the load impedance is increased, which is quite different from behaviors observed in PIN diodes at low input optical energy. This can be explained with the help of the model shown in Figure 7 and the similar reasoning used above. For a diode switch with a dynamic resistance R_d which is much less than the line impedance Z_o, the rise time of the output voltage (or current) depends on how fast the capacitor formed by the ionized dopants can be discharged. In other words, the time averaged value of $R_d C_d$ will determine the time for the collapse of the internal electric field. However, the dynamic resistance itself depends on the instantaneous value of the output current, which in turn increases with the load impedance. (Equivalently speaking, the accumulation rate of the net charges at the surfaces shown in Figure 4 can be enhanced by increasing the output impedance.)

It would be interesting to compare the drift time to separate the carriers and the R_dC_d. With the help of the model shown in Figure 4, one can roughly estimate the drift time t_a needed to separate the carriers as:

$$t_a = \frac{C_s}{NV_s} \tag{15}$$

where C_s is the surface dopants concentration, V_s is the saturation velocity of carriers and N is the concentration of electron-hole pairs generated by the laser pulse. For the 50 Ω case in Figure 6, a value of $3 \times 10^{17} cm^{-3}$ is obtained for N and $10^{11} cm^{-2}$ for C_s. This corresponds to a value of 0.33 psec for t_a, while the RC time constant estimated from the photoconductance (at 50 μJ) of this diode is around 1.3 psec. On the other hand, the output response shown in Figure 6 has a rise time of 1.3 psec.

Table 2 summarizes the output power from the diode switch at two input optical energy levels and at different load impedance. These simulated data indicate that, in order to achieve output power in the GW range, the input laser pulse energy should be in the 100 μW range and the load impedance should be smaller than 1 Ω. However, in this limit, the rise time of the output current would be slow. (The data point at 5 μJ and 1 Ω is missing as output rise time is too long and the output voltage has not reached the steady state.)

	5 μJ	50 μJ
50 Ω	3	3.1
10 Ω	10	15
1 Ω	---	100

TABLE 2. Power output (MW) at various load impedance and input energy.
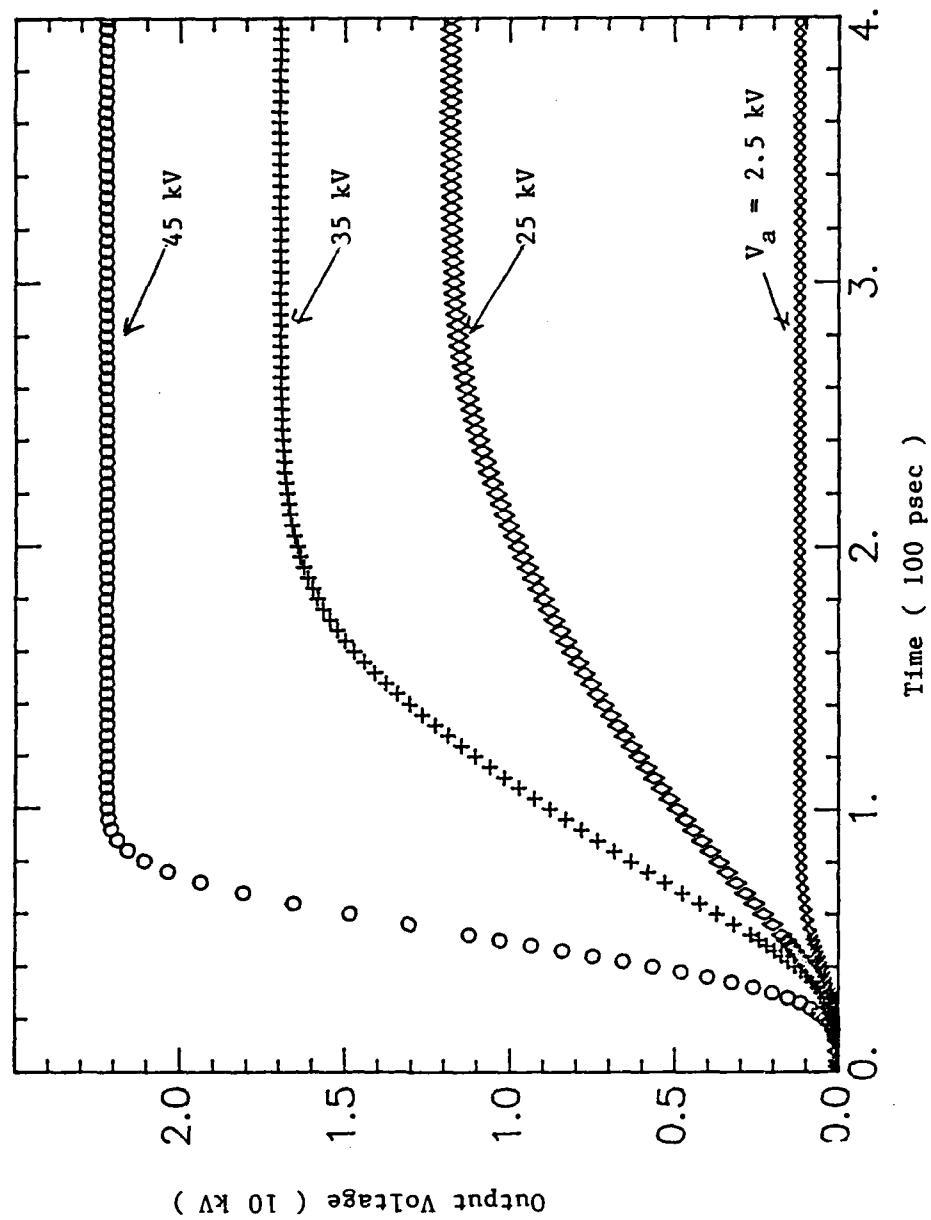
Figure 8   Simulated time response of the diode at different applied voltage;
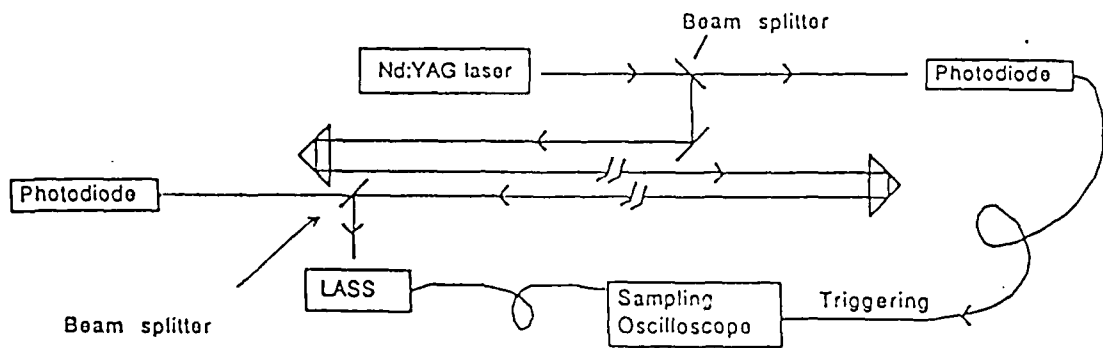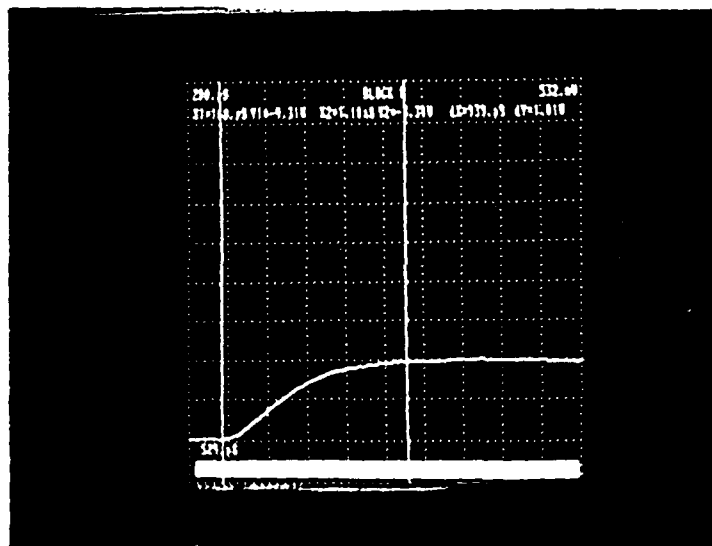the input optical energy is 5 μJ.

Figure 9   The experimental set up for measuring the characteristics of the diode switch. The second beam splitter is to monitor the laser energy.

## 5.4 Effect of avalanche multiplication on switch performance.

Next, the effect of the avalanche multiplication on the rise time of the diode switch is investigated. Intuitively speaking, the avalanche multiplication can reduce the rise time in much the same way as photo-generated carriers. For high voltage switching, from the above discussion, a high energy optical pulse is required to switch on quickly the diode switch due to the large number of the electron-hole pairs needed to cancel out the applied electric field. With the help of the carrier multiplication process through impact ionization, the dependence on the input optical energy can eb relaxed. Figure 8 shows the time response of the diode switch at different bias voltages at fixed input optical energy. Initially, the rise time increases (from 50 psec to 200 psec) as the applied voltage is increased (from 2.5 kV to 25 kV). However, once the voltage corresponding to the on-set of the avalanche is reached (around 30 kV), further increase in voltage lead to a reduction of the rise time (to 60 psec at 45 kV).
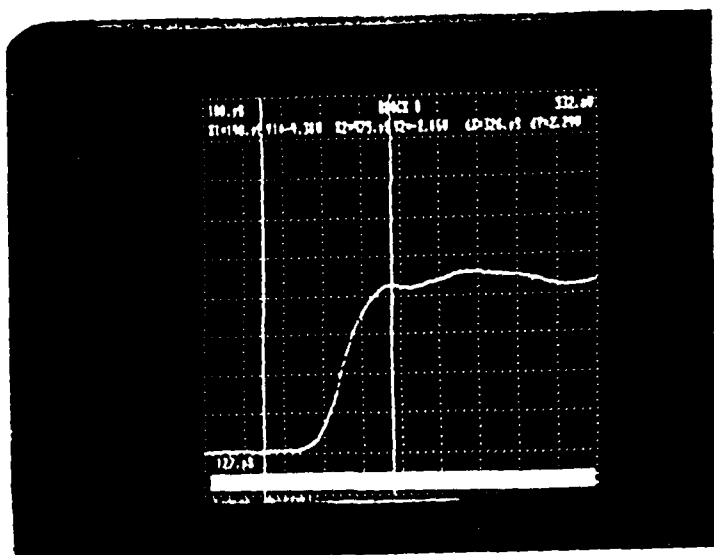
VI. Experimental Results

The predicted trend of the rise time of diode switches is verified experimentally by varying the input optical energy level. The experimental set up for this measurement is described in details in Chapters 4 and 5 of Appendix 1 and reference 1, therefore it is only briefly mentioned here. The set-up is schematically shown in Figure 9, where a mode-locked Nd-YAG laser is used to generate optical pulse with energy ranged from μJ to mJ and a pulsewidth of about 30 ps. Since the output energy of the laser fluctuate quite a bit during the measurement period, beam splitters with known power dividing ratio is employed so that the instantaneous energy level to the diode switch can be measured. Nevertheless, two difficulties persist in the measurement. Firstly, the beam profile cannot be measured accurately and consequently part of the beam falls outside the light absorption region of the diode. The results in an over-estimation of the optical energy intake by the diode and an under-estimation of the overall efficiency of the device. Secondly, for achieve lower optical energy, at first beam splitter with large power dividing ratio is used, however, the accuracy of energy measured is impaired at large ratio. This
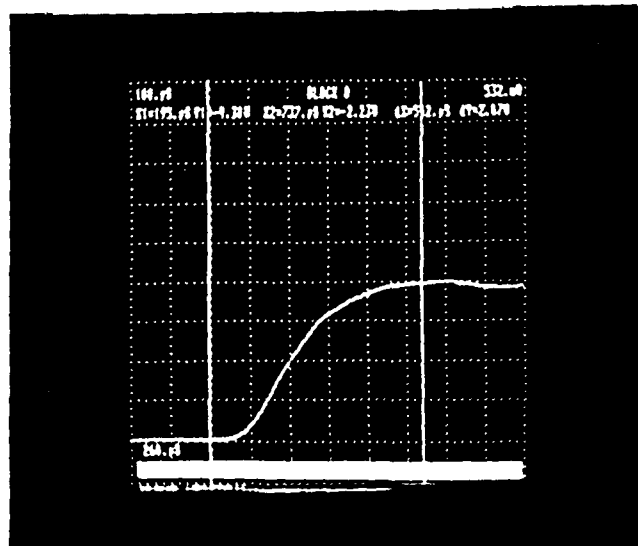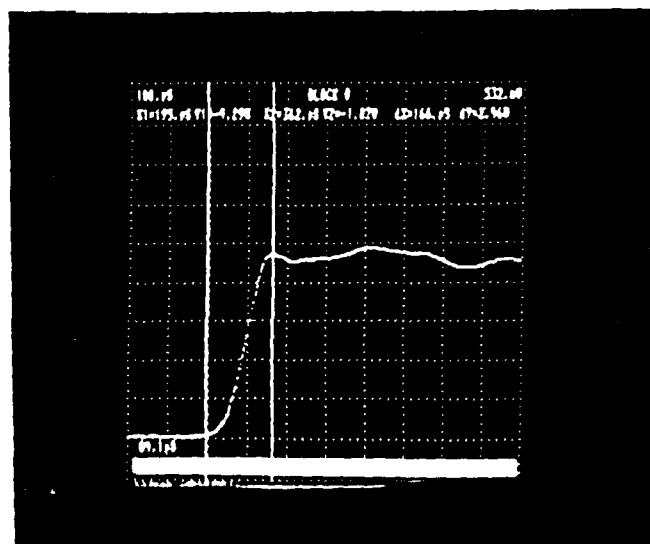
Figure 10   Experimental output rise time of a diode biased at 2500 V and at
             different input optical energy levels
             (a) 6 μJ, (b) 29 μJ, (c) 88 μJ, (d) 536 μJ.   The results are
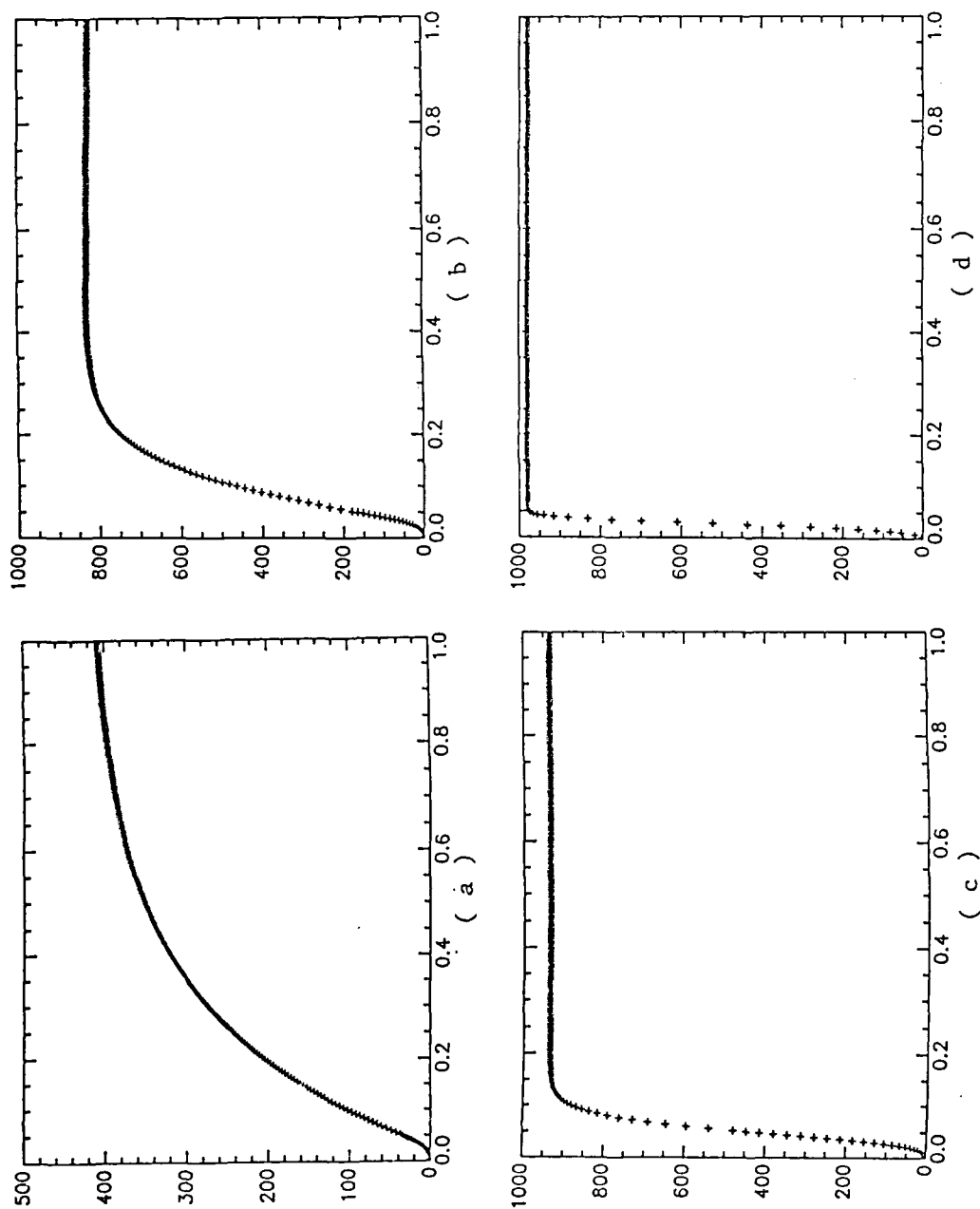   tabulated in Table 3.

Figure 11   Simulated response of the diode whose actual response is shown in Fig. 10. The horizontal scale is time (100 psec), the vertical scale is voltage output (V). The input energy to the program are (a) 0.19 μJ, (b) 1 μJ, (c) 2.9 μJ, (d) 18 μJ.

can be improved with neutral density filter placed before the diode switch. The diode switches used in these measurements are silicon PIN diodes with similar carrier concentration profiles and geometry as those used in the simulation, namely those in Figures 3, 5, and 6. In the experiment, for convenience, the transmission line impedance is chosen to be 50 Ω[6]. For diodes with 0.13 cm^2 area, the experiment was not so successful due to the power fluctuation of the laser during the measurement. The averaged rise time, however, decreases with increasing laser pulse energy, as predicted in the simulation. For diodes with 0.5 cm^2 area, the experiment was carried out with all the set up mounted on the same optical table to reduce the energy fluctuation. Figure 10 (a)-(d) shows the output responses of the diode switch at different optical energies; the rise time is summarized in Table 3. When compared to the simulated results with the same device parameters, an agreement is reached between the experiment and simulation, however, instead of unity photo-quantum efficiency for the diode, the actual value used in the simulation is only 3%. This leads to the suspicion that, during the experiment, a large portion of the light beam is wasted. The cause of the low efficiency is still a subject of current investigation

Energy (μJ)	6	29	88	536
Rise time (psec)	527	183	105	84
Voltage (V)	413	846	915	1005

TABLE 3. Rise time and output voltage versus laser energy.

Figures 11 (a) to (d) shows the simulated response to the case shown in Figs. 10 with a photo-quantum efficiency of 3%.

Although we have not performed the measurement on the rise time dependence on the load impedance, an earlier work by Zucker et al.[7] clearly suggests that the trend predicted by the

simulation is correct.

VII. Conclusion

In summary, we have developed, under this research program, a model to describe the carrier dynamics of the semiconductor diode switch excited with high energy laser pulses and interacting with an external load. The computer program developed is accurate and versatile in that both low level and high level optical excitations as well as low and high applied bias conditions can be described with ease. The transient behavior of the diode switch at different optical energy levels is understood in terms of the time to cancel out the electric field inside the diode, in contrast to the conventional transit time concept which accounts much of the behavior of the photodiodes at low bias and at low optical excitation. This behavior was confirmed experimentally. The power output of the diode switch at different transmission line impedance is investigated with this model. It is found that, the rise time of the diode can be reduced by increasing the line impedance, which agrees with experimental results obtained in an earlier work. Furthermore, high optical excitation energy and small line impedance are effective means to generate high power electrical pulses. We have made a preliminary investigation of the effects of avalanche multiplication on the performance of the diode switch and further work is needed to explore the potentials of diode switches at very high electric fields.

The findings in this work will be submitted to a refereed journal for publication.

Project Participants

University of California at San Diego -- P. K. L. Yu (PI); C. K. Sun; J. O. Bark; V. D. Lew.

Energy Compression Research Corporation -- D. Giorgi; J. R. Long; O. S. F. Zucker.

References

1. D. Giorgi, P. K. L. Yu, J. R. Long, V. D. Lew, T. Navapanich, and O. S. F. Zucker, *J. Appl. Phys.*, **63,** 930 (1988).

2. S. M. Sze, *Physics of Semiconductor Devices,* (John Wiley & Sons, New York, 1981), p. 46.

3. G. E. Stillman and C. M. Wolfe, *Semiconductor and Semimetals,* **Vol. 12,** P. K. Williardson and A. C. Beers, Eds., (Academic Press, New York, 1977).

4. D. P. Schinke, R. G. Smith, and A. R. Hartman, *Photodetectors in Semiconductor Devices for Optical Communication,* H. Kressel, Ed., (Springer-Verlag, Berlin, 1980), Chapter 3.

5. T. P. Lee, C. A. Burrus, K. Ogawa, and A. G. Dentai, *Electron. Lett.,* **17,** 431 (1981).

6. Energy Compression Research Corporation felt that experiments performed at low line impedance (say 1 Ω and below) are too classified for the University Program.

7. O. S. F. Zucker, J. R. Long, V. L. Smith, D. J. Page, and P. L. Hower, *Appl. Phys. Lett.,* **29,** 261 (1976).

UNIVERSITY OF CALIFORNIA, SAN DIEGO

Electrical Pulse Generation

through Light Activated Silicon Switches

A thesis submitted in partial satisfaction of the

requirements for the degree Master of Science

in Electrical & Computer Engineering (Applied Physics)

by
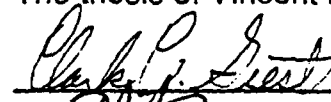
Vincent D. Lew

Committee in charge:

Professor Paul K. L. Yu, Chairman
Professor D. Asoka Mendis
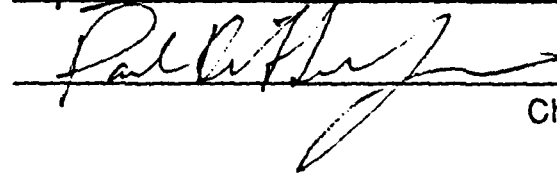Professor Clark Guest

1988

The thesis of Vincent D. Lew is approved:

_____

_____

_____
                              Chairman

University of California, San Diego

1988

Dedication

To my parents, for their support throughout my studies.

Table of Contents

Table of Contents

List of Figures

List of Symbols

C_d, differential junction capacitance (F)

c', group velocity in transmission line dielectric (cm/s)

d, width of LASS (cm)

ε, transmission line dielectric constant (F/cm)

$e(t)$, optical field (V/cm)

E, electric field across junction (V/cm)

E_c, bottom of conduction band (eV)

E_g, band gap energy (eV)

E_t, impurity energy level within band gap (eV)

E_v, top of valence band (eV)

G, gain of pulse energy over optical energy

h, thickness of transmission line dielectric (cm)

$h\nu$, photon energy (eV)

J, current density in LASS (A/cm^2)

η, quantum efficiency

I_p, photocurrent (A)

I_{ph}, primary photocurrent (A)

L, length of charged transmission line (cm)

l_n, length of depleted region on n-side (cm)

l_p, length of depleted region on p-side (cm)

List of Symbols

N_A, acceptor concentration in p region (/cm^3)

N_D, donor concentration in n region (/cm^3)

N_s, number of states from conduction band edge to arbitrary energy level (/cm^3)

n, carrier density (/cm^3)

P, switch power density (W/cm^2)

P_v, volume power density (W/cm^3)

P_{opt}, optical power incident on photoconductor (W)

R, carrier recombination rate (/s)

t_r, carrier transit time (s)

τ, carrier lifetime (s)

V, potential difference across junction (V)

V_d, built-in potential of p-n junction (V)

v_d, drift velocity (cm/s)

W, length of LASS (cm)

$W_{1 \to 2}$, transition rate of electrons from state 1 to 2 (/s)

$W_{\mu w}$, output pulse energy (J)

W_{ph}, input optical energy (J)

Z_o, characteristic impedance of transmission line (Ω)

Acknowledgement

ABSTRACT OF THE THESIS

Electrical Pulse Generation

through Light Activated Silicon Switches

by

Vincent D. Lew

Master of Science in Electrical & Computer Engineering
(Applied Physics)

University of California, San Diego, 1988

Professor Paul K. L. Yu, Chairman

In the past electrical pulses have been generated by various methods. The production of such pulses at megawatt power and nanosecond duration has yet to be realized practically. One possible solution is pulse generation by means of light activated silicon switches (LASS). Electrical energy is compressed on a transmission line and then released in the form of a pulse when the LASS is irradiated by $1.06\mu m$ light from a Nd-YAG laser. The LASS is fabricated from silicon junction devices through available semiconductor technologies. The electrical pulses are measured in real-time by conventional means and also by a sampling technique using a unique triggering scheme. Pulses with a current density of $10kA/cm^2$ and a risetime of 200ps have been demonstrated through experiments.

CHAPTER 1: INTRODUCTION

Energy compression in time and space can be acheived by various methods. The history of technology is filled with inventions demonstrating this concept. Striking a nail with a hammer is a crude example. When a hammer is accelerated it acquires kinetic energy. This energy is transferred to the nail in a time much shorter than the time it takes for the hammer to acquire the energy originally. Thus, the energy is compressed in time. Since the energy is released over the small area of the nail-head, energy compression also occurs in space. Of course, not all of the energy is transferred to the nail in the manner that is desired, some energy is lost through heat and some remains in the hammer.

Energy compression can also be facilitated by means of a switch. In this case the energy to be compressed is the electrical energy. The switch in its "off" state allows energy to be stored. Going to the "on" state the switch releases the energy so that it is compressed in time and space. The end result is the generation of a high power, short duration electrical pulse. A physical embodiment of this forms the focus of our research. Specifically, the switch is a reverse biased junction photodiode which joins two transmission lines. One of these transmission lines is charged while the switch is "open". Then irradiation of the photodiode closes the switch, allowing the compressed energy to be released, through the switch and down the second transmission line.

In chapter 2, information is given about energy compression, and optoelectronic switches such as the photoconductor and the

photodiode. Research issues and important concepts are discussed in chapter 3. Chapter 4 contains a description of how the photodiode is prepared for experimentation and the measurement procedures. Finally, results are discussed in chapter 5 concerning the electrical pulse waveform, the current density, and the risetime.

CHAPTER 2: ENERGY COMPRESSION WITH SEMICONDUCTOR OPTOELECTRONIC SWITCHES

2.0 THEORY

The subject of this thesis touches upon many fields and this chapter provides some relevant background information. In the first section we consider the generation of high-power short pulses and its importance to this study. Later sections provide some background concerning switching elements such as the photoconductor and the junction photodiode. With the high electric fields present in these devices, light-generated carriers will travel at nearly the saturation velocity so high switching speed is possible. Therein lies the importance of these two optoelectronic devices. High switching speed can be a relevant factor in the generation of electrical pulses.

2.1 HIGH-POWER SHORT PULSES

High-power short pulses are generated through energy compression by the use of a suitable switch. Switching involves a rapid change in conductivity from an "off" state (low conductivity) to an "on" state (high conductivity). In the "off" state the switch is open, and allows energy to be stored or compressed. The higher the electric field the switch can handle, the more energy can be stored. When this switch closes ("on" state) the energy is released. The greater the current density that can safely pass through the switch, the more energy per unit time and per unit area can be released since the voltage height of the pulse multiplied by the

current density will give this quantity. In general, high power handling capacity means a switch can hold a large electric field and pass a large current density. A fast switch insures the energy released is compressed in time, and not bled off slowly. These issues will be considered in more detail in the next chapter.

The major switch characteristics of interest for energy compression are its power handling capacity, switching time, and operation lifetime. An ideal switch would be able to go from zero conductivity to infinite conductivity instantaneously, be able to handle any level of power, and have an infinite lifetime. The goal of previous research by other workers has been to approach the ideal switch. Switching with a spark gap can handle high power and has good speed, but does not have a long lifetime [5]. Thyratron tubes have a long life and good speed, but low power capability [6]. Semiconductor devices such as transistors and thyristors have high power handling capacity and long lifetime [7]. However, they are limited in switching speed. In this case carriers are injected from a forward biased p-n junction into a depletion region to close the switch. The electric field in the depletion region collapses due to the presence of the first injected carriers. For low currents these carriers are sufficient to close the switch, but high currents require more carriers. The remaining carriers must travel to the depletion region by diffusion in the absence of the electric field. This slow diffusion process is responsible for the limited speed. This speed disadvantage may be overcome through the generation of carriers in the depletion region through photon absorption. The electric field will collapse as enough carriers are generated by this

process, but since diffusion is not necessary here, further carrier generation is unimpaired. The assumption here is that all of the carriers necessary to close the switch are generated within the depletion region. Given a laser that delivers light pulses of sufficient power this assumption is acceptable. Thus, we need not consider the effect of carriers created outside the depletion region which would require diffusion to reach the depletion region. The importance of employing junction semiconductors with light activation has only recently been recognized. Adding the feature of high switching speed when light activation is employed to the other semiconductor device characteristics (high power handling capacity, long lifetime) the resultant light activated silicon switches (LASS) have the potential advantage over any other competing process [1].

To produce square pulses with reduced pulsewidth, short risetimes are necessary. Faster risetimes go hand in hand with greater switching speed as the ideal switch is approached. In general the risetime should be an order of magnitude smaller than the pulse length. For example, a 1ns square pulse should have a risetime less than 0.1 ns. Also, the pulses can be timed more accurately with respect to each other if there is a faster risetime. In other words, if one pulse is followed by another which has a certain risetime, then there is an uncertainty in the interval between the two pulses at least equal to the risetime. Decreasing the risetime will reduce the uncertainty.

A source which generates high-power short pulses finds utility in many areas. An antenna array of these sources can

produce a microwave burst when individual antennae are properly timed. The direction may then be controlled through phased array techniques. High-power short pulses can be used to provide information about low-density photo-induced plasmas in semiconductors. Other applications are found in the jitter-free streak camera and prepulse suppression in laser fusion [2].

2.2 PHOTOCONDUCTOR

In this section an understanding of how the photoconductor works will be provided. Such an understanding provides a comparative basis for the photodiode which is the essential device investigated in our research. Electron-photon interaction can occur through three basic processes in matter: Spontaneous emission, stimulated emission, and absorption. The process of absorption is the main concern when dealing with the photoconductor. When an electron absorbs a photon of sufficient energy the electron may transition from an initial state to a final state where the electron is free to move and, thus, contribute to the external current. An intrinsic transition involves the movement of an electron from the valence band to the conduction band (figure 2.1). The energy absorbed must be equal to (or greater than) the band gap energy ($h\nu \geq E_g$). In figure 2.1 transition (a) involves the absorption of energy exactly equal to the band gap energy while transition (b) involves a greater energy. Here the excess energy is dissipated as heat. An extrinsic transition (c) involves a transfer of an electron from the valence band to a state within the band gap. This transition can
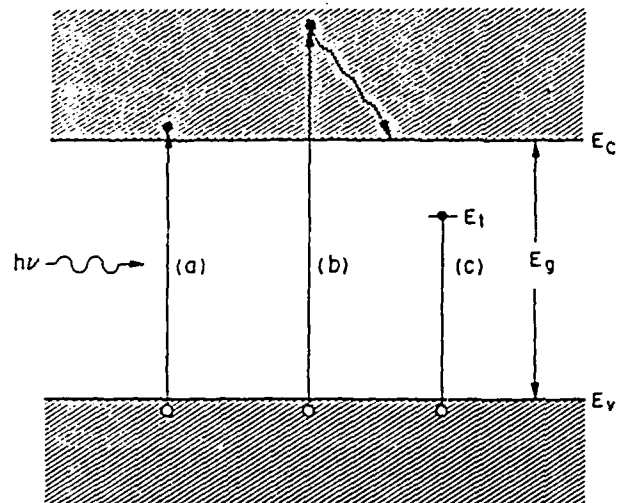
FIGURE 2.1 Electron transitions through the band gap [Ref.4].
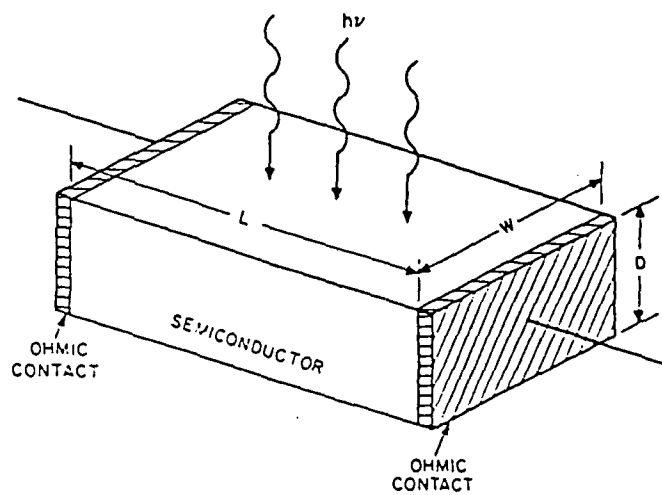
FIGURE 2.2 Photoconductor switch [Ref.4].

occur only if the semiconductor has an electronic state within the band gap due to physical defects or impurities. Photon absorption, in all three cases, is accompanied by the generation of an electron-hole pair. A hole carrier also contributes to the current.

Due to absorption, the photon flux will decrease exponentially with distance as it moves through a semiconductor provided the photons have an energy greater than the band gap. From elementary quantum mechanics the transition rate ($W_{1->2}$) of electrons between the initial "1" and final "2" state can be related to the optical field e(t) through the following:

$$W_{1->2} \sim \underline{E}(t)\underline{E}^*(t) \quad (2\text{-}1)$$

$$e(t) = Re[\underline{E}(t)] \quad (2\text{-}2)$$

where $\underline{E}(t)$ is a complex function whose real part is the optical field function. From $\underline{E}(t)$ information can be determined about the transition rate.

Photoconductive switches have been investigated for switching electrical energy. A schematic diagram of a photoconductor switch is shown in figure 2.2. A semiconductor slab has ohmic contacts at its ends and has constant optical flux incident on it. The light generates electron-hole pairs through intrinsic or extrinsic transitions. For n-type semiconductors extrinsic transitions involve an impurity level (donor) close to the conduction band edge while for p-type semiconductors the impurity level (acceptor) is close to the valence band edge. The generated carriers drift under the influence of the applied electric field until recombination occurs or the carriers pass into the external circuit.

The presence of these carriers will lower the resistance across the semiconductor slab and contribute to the external current. At steady state the generation rate G must equal the recombination rate R plus the rate of those carriers lost to the external circuit, and then if we assume the penetration depth to be less than the thickness,

$$R = \frac{n}{\tau} \qquad (2\text{-}3)$$

$$G = \frac{\eta(P_{opt}/h\nu)}{LWD} \qquad (2\text{-}4)$$

where n is the carrier density; τ is the carrier lifetime; and L is the length, W is the width, and D is the thickness of the semiconductor slab. The photocurrent I_p is related to the primary photocurrent I_{ph} through the gain G_n by

$$I_p = I_{ph} G_n \qquad (2\text{-}5)$$

$$I_{ph} = q\left[\eta\frac{P_{opt}}{h\nu}\right] \qquad (2\text{-}6)$$

$$G_n = \frac{\tau}{t_r} \qquad (2\text{-}7)$$

where η is the quantum efficiency, P_{opt} is the incident optical power, $h\nu$ is the photon energy, and t_r is the carrier transit time. More complete information concerning the photoconductor may be found in various textbooks [3,4].

2.3 JUNCTION PHOTODIODE

The photodiode operating as a switch is the device to be investigated in our experiments. This section will provide some basic information on the photodiode. Essentially the photodiode is a reverse biased p-n junction. The p-n junction is formed in a semiconductor material when the dominant doping type is changed from p-type in one region to n-type in another region (figure 2.3(a)). The main carriers are electrons in the n-type region and holes in the p-type region. Figure 2.3(a) illustrates the doping profile that may be acheived through the diffusion of impurity atoms into a p-type or n-type semiconductor substrate to create an n -type region in p-type substrate or vice versa. Figure 2.3(b) is the energy band diagram of the p-n diode in the absence of any applied bias. The energy necessary to enable an electron to go from the n side to the p side in the absence of bias is eV_d, where V_d is called the built-in potential. The potential energy of an electron as a function of x is represented by the top or bottom curve in the band diagram. The energy band diagram shown in figure 2.3(c) depicts the situation when a reverse bias V_a is applied across the junction. This reverse bias causes mobile carriers to move away from the junction so that the size of the depletion region increases. Consequently the potential barrier for carrier transport becomes $e(V_d+V_a)$. Figure 2.3(d) shows the distribution of the ionized impurity atoms and

$$N_A l_p = N_D l_n \quad (2\text{-}8)$$
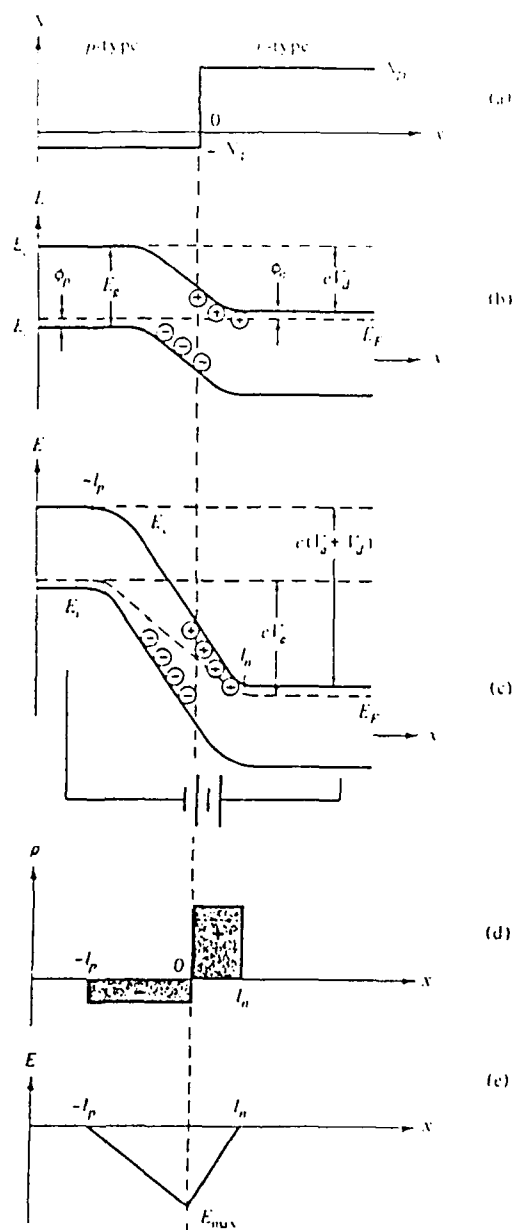
FIGURE 2.3 P-n junction: (a) doping profile, (b) energy band diagram with no bias, (c) energy band diagram under reverse bias, (d) distribution of ionized impurity atoms, (e) electric field versus distance [Ref.3].

where l_p and l_n are the lengths of the depleted regions on the p-side and n-side, respectively, so that the positive and negative charge are balanced in the depletion region. Relations for the electric field, the potential, and the depletion lengths can be found in the literature [3,4]. The electric field as a function of distance is shown in figure 2.3(e). Across the junction is a differential capacitance per unit area C_d

$$\frac{C_d}{AREA} = \frac{\varepsilon}{l_p + l_n} \quad (2\text{-}9)$$

When an optical intensity falls on the junction photodiode, certain processes may occur and contribute to the external current (figure 2.4). In process "B" the electron-hole pair is generated within the depletion region. The electric field then separates them so that the electron and hole move in opposite directions contributing to the external current. In process "A", an electron-hole pair is generated in the p region. If this pair is within a diffusion length from the depletion region edge, then the electron has a good chance of reaching the depletion region. Of course, the hole is prevented from moving into the depletion region, because of the potential barrier. Once the electron is in the depletion region, the electric field will cause the electron to drift across and contribute to the current. The same can be said about the hole in process "C". Although here, the hole moves in the opposite direction. To obtain a high quantum efficiency (number of carriers flowing in the external circuit for each incident photon), the "B" process must dominate, because in the other two processes,
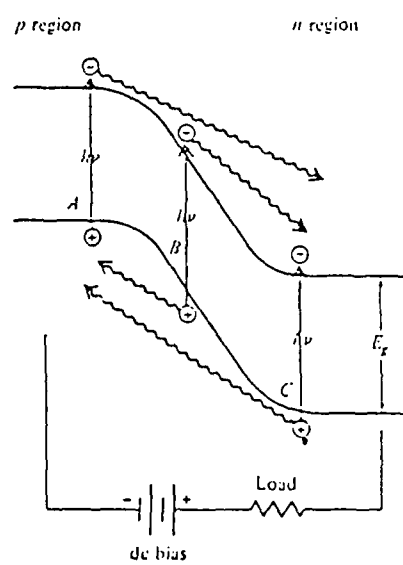
FIGURE 2.4 Electron-hole generation in a photodiode [Ref.3].

a large portion of the carriers does not reach the depletion region. Thus, a large depletion region is beneficial. This increases the transit time across the depletion region and reduces the frequency response of the photodiode. Thus, there is a tradeoff between quantum efficiency and frequency response. The diffusion time in processes "A" and "C" also limits the frequency response as does the shunt capacitance. In fact, if the depletion region is made small enough the junction capacitance can become large in value (see above equation 2-9), affecting the frequency response to a significant degree. When the transit time across the depletion region is approximately one half the modulation period of the optical signal the best compromise is reached between quantum efficiency and frequency response. Various texts have a more detailed treatment of the ideas discussed above [3,4].

2.4 CONCLUSION

In this chapter the basic processes involved in a photoconductor and photodiode have been explained so that the experiments in energy switching with the photodiode can be better understood. There are important differences between photoconductors and photodiodes. For photoconductors the voltage holding capacity in the "open" state increases with increasing "gap" width (located in the section of the semiconductor where light is irradiated to close the switch), while 15kV is the typical value for photodiodes. However, the "open" state voltage for photoconductors cannot remain for longer than 10ns. Otherwise thermal runaway will occur because of its current leakage in the "open" state.

Junction photodiodes are the better choice for experimentation since the technology involved in their manufacture is already well established. In addition, the junction semiconductor switch has desirable qualities of high power handling capacity and long operation lifetime, and with light activation it is expected to have high speed. This device then is the focus of our research. In the next chapter, we will see how the junction photodiode enables the compression and release of electrical energy, and various specific research issues of concern will be discussed.

References:

1. Zucker, O., "Light Activated Semiconductor Switches," Preprint UCRL-80046 for submission to the Seminar on Energy Storage, Compression and Switching, Canberra, Australia, November 15-21, 1977.

2. Mourou, G., W. Knox, S. Williamson, "Advances in Picosecond Optoelectronics," SPIE Picosecond Lasers and Applications, vol.322, pp.107-114, 1982.

3. Yariv, A., Optical Electronics, New York: Holt, Rinehart and Winston, 1985, Ch.11.

4. Sze, S., Semiconductor Devices, Physics and Technology, NewYork: Wiley, 1985, Ch.7.

5. Odom, H., T. Burkes, "High Power Switch Capabilities," Second International Conference on Energy Storage, Compression, and Switching, Venice, Italy, December 5-8, 1978.

6. Menown, H., "Gaseous Switches: The Past and Present State of the Art," Proceedings IEEE International Pulsed Power Conference, Lubbock, Texas, November 9-11, 1976.

7. Pittman, P., D. Page, "Solid State High Power Pulse Switching," Proceedings IEEE International Pulsed Power Conference, Lubbock, Texas, November 9-11, 1976.

CHAPTER 3: RESEARCH ON THE GENERATION OF PULSES THROUGH THE LASS

3.0 INTRODUCTION

A junction semiconductor device joined onto a transmission line is a novel approach to generating pulse power. As mentioned in the previous chapter, junction devices switched by light activation have an advantage in speed over other junction semiconductor devices while retaining the characteristics of high power capability and long operation lifetime. Section 3.1 presents important definitions and concepts useful in our investigation. Section 3.2 discusses those areas of research that concern this project.

3.1 DEFINITIONS AND TERMINOLOGY

In our experiments energy compression is acheived through a Light Activated Silicon Switch (LASS) and a transmission line (figure 3.1). The left side is charged up to a voltage over several milliseconds while the LASS is open: Energy is stored. Then the LASS is closed when light shines on it, allowing a square pulse of nanosecond duration to propagate down the line: Energy is released, having been compressed in time and space.

Figure 3.2 is a representation of the LASS and transmission line from which certain definitions will be obtained. Absent from this picture is the transmission line dielectric between the top and bottom conductor. If the left side is charged to a voltage V and has a length L, then the pulse generated will have a voltage height V/2
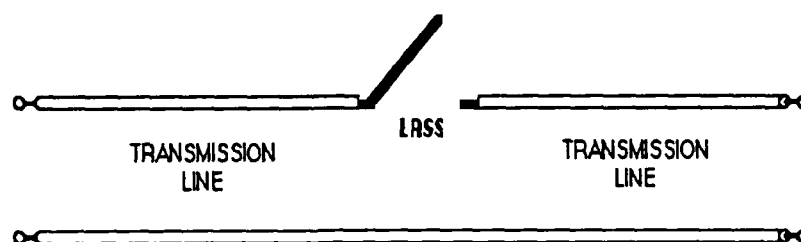
FIGURE 3.1 Schematic of LASS-transmission line
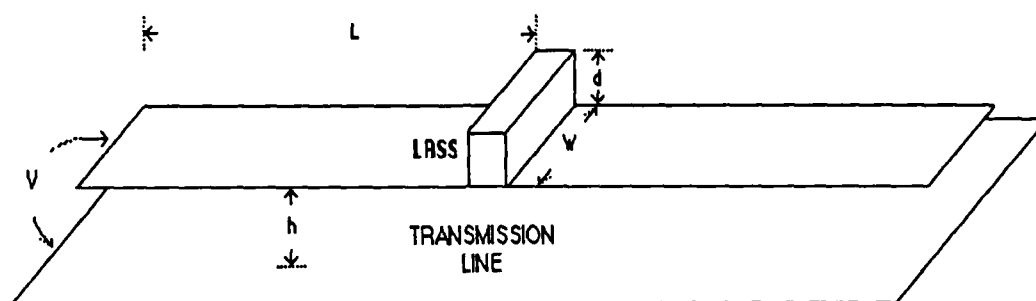
FIGURE 3.2 Physical representation of LASS-transmission line
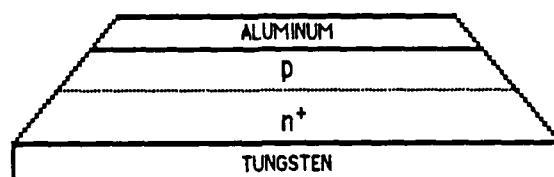
FIGURE 3.3 LASS internal structure

and a duration of 2L/c' (c'=group velocity in the dielectric), because as the LASS closes, the standing wave form of the voltage can be resolved into two pulses, one going forward and the other backward, each with a pulsewidth of L/c' and a voltage V/2. The backward pulse reflects off of the open circuit at the left end and joins with the tail end of the forward pulse to produce one pulse of duration 2L/c' (as a rule of thumb, which we will find useful in section 5.3, one nanosecond is approximately equivalent to one foot divided by the square root of the dielectric constant).

For a transmission line of characteristic impedance Z_o matched to the LASS, the current density J is

$$J = \frac{V/2}{Z_o} \left(\frac{1}{Wd} \right) \qquad (3\text{-}1)$$

and from Boltzmann transport theory, assuming medium electric field strength, the current density in the switch is

$$J = n_e e v_d \qquad (3\text{-}2)$$

where n_e is the carrier density , e is the electron charge, and v_d is the drift velocity. High current density which leads to high power density (see equation 3-3) is desirable in pulse power applications. A generator of high power pulses can be made smaller in size if it is characterized by high power density, because a small device with high power density can generate the same power as a large device with low power density. For example, a source characterized by a power density of $0.25 MW/cm^2$ with an area of $4 cm^2$ can deliver a power of 1MW, while the same power results from a smaller device with an area of $1 cm^2$ if its power density is

$1MW/cm^2$. Thus, an array of these generators will correspondingly be reduced in size. The switch power density P (power/area) is

$$P = V \times J \qquad (3\text{-}3)$$

and the volume power density P_v (power/unit volume) is

$$P_v = E \times J \qquad (3\text{-}4)$$

with V and E the potential difference and electric field across the junction device, respectively. Typical values for a thyristor will show the high power capability of semiconductor materials. A thyristor can carry a current density of $10kA/cm^2$ and its electric field can exceed $100kV/cm$. Thus, the volume power density can have a value of $1 \times 10^9 W/cm^3$.

The ratio between output pulse energy $W_{\mu w}$ and optical input energy W_{ph} is the gain G

$$G = \frac{W_{\mu w}}{W_{ph}} \qquad (3\text{-}5)$$

If a joule of laser light ($W_{ph}=1J$) is absorbed at the 1.0 eV band gap of silicon, then approximately one coulomb of charge will pass across the depletion region. In other words, each photon will create an electron-hole pair and these two carriers will move in opposite directions. The distance that each carrier travels through the depletion region, when added together, will equal the length of the depletion region. Then this will be equivalent to one electron traveling the entire length of the depletion region as far as the external current is concerned. Since 1J creates 1.6×10^{19} electron-hole pairs, this is equivalent to the same number of

electrons (1 coulomb) crossing the depletion region. A coulomb of charge, dropping through a potential of 5kV across the depletion region (open circuit switch voltage) will gain an energy of 5kJ ($W_{\mu w}$=10kJ). Then the gain G can be as high as 5×10^3(5kJ/1J) according to the equation (3-5). This illustrates the large gain possible with the LASS when a typical value of the breakdown voltage is considered. However, in order for the LASS to absorb 1J of light the device volume must become larger than is desired as far as the current density is concerned: Increasing the volume will increase the area through which the current flows, thus reducing the current density possible. In fact only a small fraction of the light available will be absorbed (see Section 5.2), for the actual size of the device used in our experiments.

Since only low impedance transmission lines (h<<W, see figure 3.2) are used in our experiments, the characteristic impedance Z_o may be found through the approximate expression

$$Z_o = \frac{120\pi}{\sqrt{\varepsilon}} \frac{h}{W} \qquad (3-6)$$

where ε is the dielectric constant of the transmission line [1].

The structure of the present LASS is shown in figure 3.3. A p-n$^+$ silicon junction device has an aluminum coating on the p side and a tungsten contact on the n$^+$ side. The sides are beveled and passivated with silicon dioxide to prevent high voltage breakdown (see section 4-1). The 1.06μm wavelength infrared light matched closely to the silicon band gap enters the junction through the sides and when absorbed, generates carriers. The LASS has the

potential to hold a maximum reverse bias of 1-5kV *depending on* the manufacturer's specification of the power diode from which the LASS is cut. The leakage current ought to be no more than a few microamperes at 1kV to prevent the LASS from thermal runaway. Thermal runaway involves a cycle of increasing heat dissipation in the device. If the power dissipated as heat (product of the leakage current and the voltage) is great enough to raise the temperature of the device so that the leakage current is increased, then even more heat is dissipated. Of course this increases the temperature further, which in turn increases the leakage current and so on. The net result is severe damage to the device.

3.2 RESEARCH TOPICS INVOLVING THE LASS

Topics of theoretical and experimental interest are the following: Establishing the maximum current density that can be handled by the LASS, light coupling into the LASS, photon absorption within the junction at high power and switching speed. For the LASS to carry a certain current density, corresponding values of carrier density and drift velocity are needed according to equation (3-2). However, at high current density, the drift velocity v_d will reach a limit so that higher current densities depend only on an increasing carrier density. Now carrier generation is impaired as carrier density is increased, because as the available *conduction* band states are filled by electrons it becomes more improbable that any one photon will be absorbed (see related discussion in section 5.2). Thus, this is a concern in maximizing current density.

Then again, when drift velocity approaches the thermal limit, avalanche gain occurs through carrier impact ionization in the junction. Avalanche gain enhances carrier generation so that a larger current density is possible. The interrelationship of these factors must be explored to discover the limits to current density. Of course from equation (3-1) high current densities may be investigated experimentally by increasing the breakdown voltage V, by decreasing the dimensions d and W, or by decreasing the characteristic impedance Z_o. There are experimental difficulties associated with changing any of these parameters [2,3].

Previously, light coupling was implemented by shining light through a hole made in the device electrodes. However, a conceivably better method is to shine light through the side surface passivation in as much as light can enter more directly into the junction. This method will be used in our experiments and it will be of interest to observe the effects of light passing through the passivation layer.

As a general rule, the absorption coefficient of a semiconductor material increases with photon energy until it comes to a constant value. However, a photon energy close to the bandgap of silicon ($\lambda \approx 1.06 \mu m$) is chosen in our experiment even though this results in an absorption efficiency below the maximum possible. The reason for this is that the absorption length must be considered. Carriers need to be generated in the entire volume of the LASS and this requires the mean absorption length to be long enough to reach into the depths of the material. Since this length

increases with decreasing photon energy (due to the availability of energy states in the semiconductor) a value of the photon energy close to the band gap energy is chosen. Slight variations in the photon energy or wavelength will allow the best value to be chosen in relation to the absorption efficiency and absorption length.

Given the preceding restriction on the aborption efficiency, the interest here is how to raise this efficiency. The material doping and the number of carriers affect the absorption efficiency to a large degree. The doping is fixed from the manufacturing process, but the number of carriers must be measured. From the current density the product of drift velocity and carrier concentration can be determined. However, the number of carriers itself is difficult to ascertain. Separating the two parameters is a subject for investigation. Observing how the absorption efficiency changes with the doping and the number of carriers will allow the maximization of this efficiency [4,5].

The speed of the LASS in going from the "off" state to the "on" state is obtained by measuring the risetime of the pulse. Important factors which limit the risetime can be the power of the light source and the impedance mismatch between the LASS and the transmission line. For each current density there must be a corresponding carrier density present according to equation (3-2). The carrier generation follows closely the laser pulse, so the power of the laser pulse can be a limiting factor. For example, in order to demonstrate a current density with a 100ps risetime the necessary carrier density must be generated in 100ps or less. As a consequence, the energy transmitted per unit time (or power of the

laser pulse) is a determining factor. As the pulse travels along the transmission line, it encounters an impedance mismatch where the transmission line meets the LASS. This mismatch increases the risetime so that attempts must be made to reduce this impedance mismatch. Under ideal conditions (elimination of the impedance mismatch and unlimited laser pulse power) the suggestion from theory is that the turn-on speed will be limited by the dielectric relaxation time ε/σ (ε is the dielectric constant and σ is the conductivity) and the photon absorption time of the semiconductor. Both of these are in the femtosecond range. Therefore, the ultimate risetime would be in the same range [6]. However, it remains to be seen to what extent this is true, and even whether or not it matters, given the limitations imposed by the impedance mismatch and the laser power.

3.3 CONCLUSION

Electrical pulses can be generated through energy compression with the utilization of a LASS and a transmission line. A quantity of interest is the current density which is dependent on the breakdown voltage of the LASS, the size of the LASS, and the impedance of the transmission line. From the current density the power density can be obtained. Also of interest is the gain which is the ratio between the output electrical energy and the input optical energy.

There are certain experimental and theoretical issues that interest us. One issue is the maximization of the current density

where the carrier generation process and the presence of avalanche gain must be considered. Laser light coupling into the LASS may be more effectively realized by entrance through the side surface passivation. The absorption efficiency can be maximized when the effects of material doping and number of carriers are studied. In addition the absorption efficiency will be limited by the need for a suitable absorption length. The speed of the LASS can depend on the laser pulse power and the impedance mismatch between the LASS and the transmission line so that these two factors must be investigated. In the next chapter we will discover what methods and procedures can be implemented to explore some of these issues.

References:

1. Gandhi, O., _Microwave Engineering and Applications._ New York: Pergamon Press, 1981, p.52.

2. Caughey, D., R. Thomas, "Carrier Mobilities in Silicon Empirically Related to Doping and Field," _Proceedings of the IEEE,_ vol.55, pp.2192-2193, 1967.

3. McKay, K., K. McAfee, "Electron Multiplication in Silicon and Germanium," _Physical Review_, vol.91, pp.1079-1081, 1953.

4. Philipp, H., E. Taft, "Optical Constants of Silicon in the Region 1 to10eV," _Physical Review_, vol.120, pp.37-38, 1960.

5. Conwell, E., "Properties of Silicon and Germanium: II," _Proceedings of the Institute of Radio Engineers,_ vol.46, pp.1281-1300, 1958.

6. Zucker, O., "Light Activated Semiconductor Switches," _Preprint UCRL-80046 for submission to the Seminar on Energy Storage, Compression and Switching,_ Canberra, Australia, November 15-21, 1977, p.3.

CHAPTER 4: LASS PREPARATION AND MEASUREMENT PROCEDURES

4.0 EXPERIMENTAL SETUP

The basic device involved in our experiments consists of a LASS joined onto a microstrip transmission line. Section 4.1 describes how the LASS is suitably prepared for use as a switch, and then assembled with the microstrip transmission line. Sections 4.2, 4.3 describes how the microstrip transmission line is prepared for experimentation. Section 4.4 describes how measurements are made and the equipment used in our experiments.

4.1 FABRICATION OF THE LASS

The LASS devices used in our experiments are cut originally from silicon power diodes with diameters ranging from 1cm to 6cm. This is done so that the lateral dimension of the LASS will be small enough to fit onto a transmission line. Before the cut is made, most of the tungsten layer which forms one of the contacts to the silicon power diode must be removed. A thin layer of tungsten is left next to the silicon surface to ensure that a good electrical and thermal contact can be made at that surface. The removal of the tungsten can be done by placing the diode on a holder such that the exposed tungsten layer side is abraided by a rotating abrasive surface.

A wire string saw (Laser Technology, Inc.) cuts the silicon diode into small rectangular pieces with a dimension of 2×4 mm^2. This saw enables clean, sharp cuts to be made without damage to the bulk material due to vibration. Diamond particles are embedded

into a wire which is drawn back and forth across the specimen to be cut, thus the wire saw cuts by an abrasive action. The wire is .008 inches in diameter and the diamond particles are 45 microns in size.

The LASS is to be operated under high reverse bias which requires beveling the sides of the LASS device and side surface passivation with SiO_2. Since the silicon power diode is manufactured with a particular breakdown voltage limit which can vary from 1000 to 5000 volts, we expect to reach these limits with the LASS. The breakdown voltage can be increased when the sides of a diode have been beveled or sloped [1]. A beveled side results in a reduction of the electric field along the silicon surface and a movement of the electric field maximum towards the low doped region. Thus, the possibility of voltage breakdown at the silicon surface over the p-n$^+$ junction is reduced. The beveled side is created by attaching the rectangular piece onto a holder with wax (figure 4.1). This holder has two adjacent sides which form an angle of 135°. The rectangular piece is placed onto side b, tungsten facing the holder, with the edge of the rectangular piece extending beyond where the holder sides meet. Then side a is passed back and forth across a grinding surface. This causes the edge of the rectangular piece to be sloped at an angle of 45°. All four sides of the rectangular piece are beveled this way. Because a 45° angle can be obtained with relative ease using the above procedure and it contributes to a breakdown voltage suitable for our present experimental purposes, this angle is chosen even though
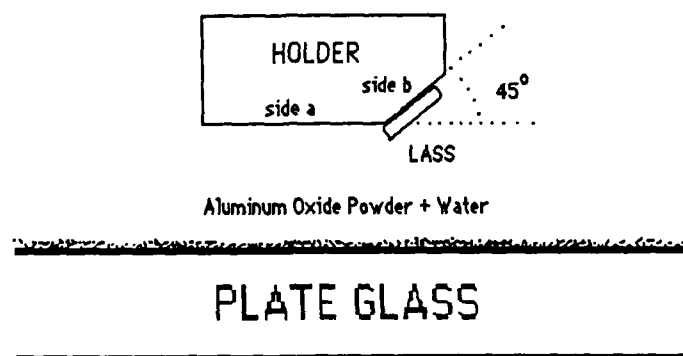
FIGURE 4.1 Beveling of the LASS

smaller angles can further reduce the surface electric field. The grinding surface consists of a glass plate onto which an abrasive powder, mixed with water, is placed. First we use a coarse grain of $10\mu m$ abrasive powder to remove most of the edge. After rinsing, a finer grain of $1\mu m$ is used to produce a shiny mirror-like surface on the silicon. Also, observation of the beveled sides under a microscope (30x) shows no noticeable fractures or cracks. This characteristic is important to prevent premature breakdown due to defects at the surface.

The rectangular piece, now beveled, must then be cleaned and etched in preparation of the passivation process. First, the rectangular piece is held by a teflon tweezer on top of a semiconductor graded paper cloth and the beveled sides are wiped by a cotton swab which has been immersed in TCE. Second, when the beveled sides have been cleaned with the TCE, the rectangular piece is immersed into acetone for several minutes. Finally, we place the rectangular specimen in methanol, also for several minutes, and from there into a beaker with running deionized water.

After the specimen is removed from the beaker, it is blown dry with nitrogen. The specimen is held by the teflon tweezer on its aluminum and tungsten contacts so that the side silicon surfaces will be fully exposed for etching. We place the specimen in an etchant for 3 seconds while continuously agitating the specimen. We then remove the specimen and immediately place it into the beaker with running deionized water. The etchant, which consists of nitric acid, hydrofluoric acid, and acetic acid (15:5:3),

can remove a very thin layer of silicon from the surface.

The specimen is removed from the water, dried by the nitrogen gun, and placed in a Chemical Vapor Deposition (CVD) reactor to passivate the beveled sides of the specimen. A SiO_2 layer is formed on the beveled sides after 10-20 minutes in the CVD. The layer is 1500 A thick when we observe a dark blue coloration in the layer. A passivation dielectric layer adjacent to the silicon surface protects it from ions in the ambients.

After the specimen has gone through the above procedure, it becomes the LASS device to be used in the experiments. The LASS is then tested with a transistor curve tracer to observe its voltage holding characteristics at high reverse bias. Voltages are applied to 1kV and for good diodes, the leakage current ought to be no more than a few microamperes. Sometimes the leakage current will be higher than this, which may be attributed to the imperfect execution of any step or steps from the above procedure.

The leakage current increases with time as the passivation layer absorbs impurities. Since a major impurity is simple moisture, a dessicant is placed inside the container storing the LASS. Even then the leakage current can degrade with time. Also, the passivation layer may be damaged after several experiments if the light pulses impinging on it are too strong. Neutral density filters can be used to minimize this effect. However, a LASS which has a damaged passivation layer may be regenerated for use in future experiments. The passivation layer is removed by placing it in a beaker filled with buffered hydrofluoric acid. After an hour

the LASS is removed from the beaker and rinsed. The LASS is then cleaned, etched, and passivated once again according to the above procedure.

4.2 FABRICATION OF THE MICROSTRIP TRANSMISSION LINE

To obtain the microstrip transmission line we take a sheet of dielectric substrate (Oak Industries and Rogers Corporation) which has a layer of copper on both sides. Most of the copper on one side is etched away so that a strip of copper remains, whose width is determined by the impedance requirement (figure 4.2), with a gap in the middle. The etchant is a ferric chloride solution which is composed of 60 grams of FeCl in 1 liter of deionized water. The region to be etched is masked with PVC tape. In the experiments a stripline obtained from Lawrence Livermore National Laboratories has also been used.

4.3 LASS-MICROSTRIP ASSEMBLY

The LASS, properly beveled and passivated, is joined onto the microstrip transmission line, as shown in figure 4.3(a). The LASS is placed in the gap and between the stripes so that one of its beveled sides is flat against the dielectric. One end of a copper strip is soldered to the upper conductor of the transmission line and the other end is held against the aluminum or tungsten contact under mechanical pressure.

Another arrangement is shown in figure 4.3(b) where the LASS is placed on one of the upper conductors, tungsten side down. One end of a copper strip is soldered to the other upper conductor
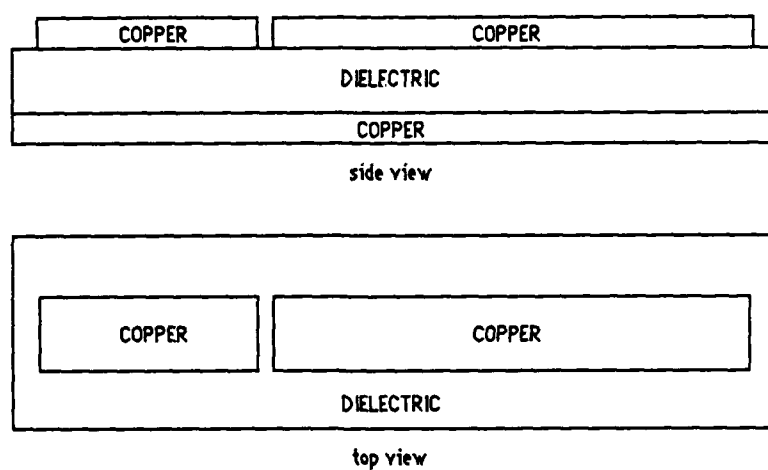
FIGURE 4.2 Microstrip transmission line

(a)

(b)
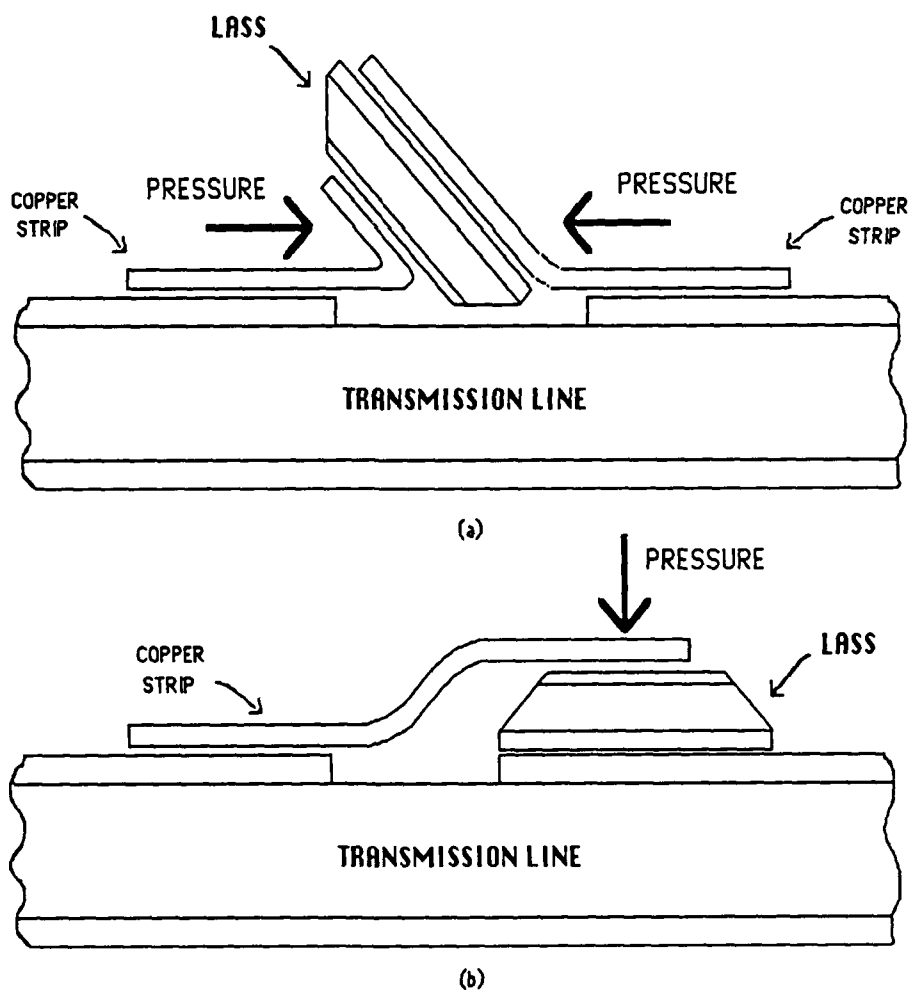
FIGURE 4.3 LASS placement into the transmission line

with the opposite end of the copper strip pressed onto the aluminum contact. To reduce the resistance between the copper strips and the aluminum or tungsten contacts, silver paint or silver paste has been applied there, but no noticeable improvement is observed.

The arrangement of figure 4.3(a) is supposed to be advantageous, because the current in the upper conductor can flow in a straight line through the LASS whereas in the arrangement of figure 4.3(b) the current must go up through the copper strip then down through the LASS. However, the square pulses obtained during switching with these two arrangements appears to be the same. Apparently, the current path is not sufficiently disturbed to cause a distortion in the waveform, at least not at the voltage and current density levels which our experiments are conducted under. Therefore, the arrangement of figure 4.3(b) is used due to its ease in implementation.

4.4 MEASUREMENT PROCEDURE

The LASS-microstrip assembly is placed into the measurement setup depicted in figure 4.4. A high voltage source (Fluke 3kV Power Supply) is applied to the LASS so that it is reversed biased. We note that the charging leads from the high voltage source are soldered onto the microstrip line on the top and bottom. Also, the leads are not soldered at the end of the microstrip line, but rather near the center of the left side in order to have a cleaner square pulse at its trailing edge. Otherwise, there is a noticeable distortion here due to a discharge off of the
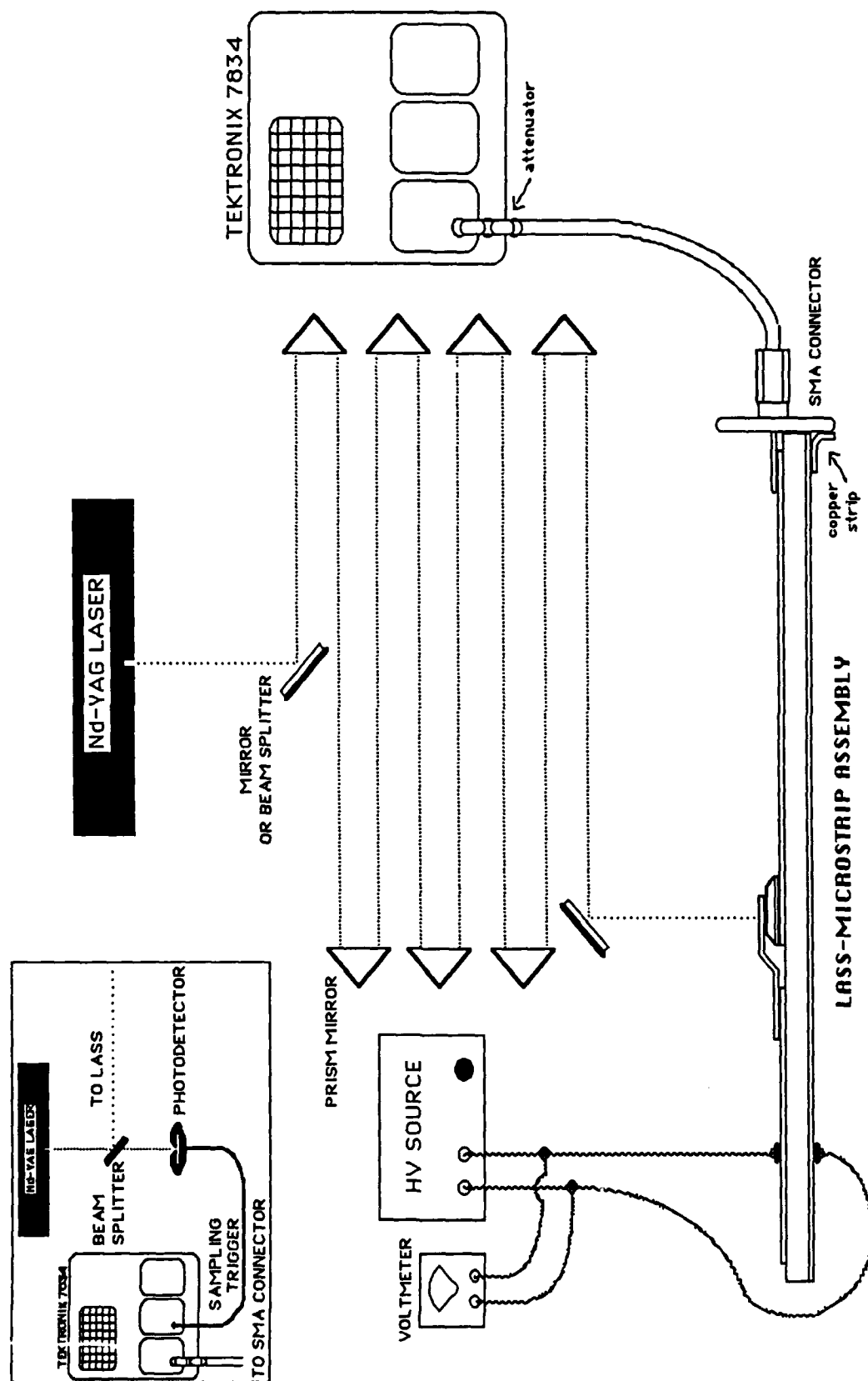
FIGURE 4.4 Measurement scheme

charging leads.

At the opposite end of the assembly we have an SMA connector (Connecting Devices, Inc). A small piece of copper connects the bottom side of the microstrip line to the outside conductor of the SMA connector (figure 4.4). A 50Ω coaxial cable is then attached to the connector with the other end going through an attenuator to a Tektronix 7834 which has a risetime of 1ns. The Tektronix 7S12 unit (risetime of 35 ps) is added on for sampling measurements. Attenuators are necessary to scale down the high voltage to a range which the oscilloscope can handle.

Sampling measurements used in this experiment require an unusual method of triggering. The leading edge of the square pulse from the LASS has a risetime below 100 picoseconds, which we want to measure. With the laser firing at a repetition rate of 10 Hz, the generated square pulses are separated by 0.1 seconds. Normally in sequential sampling, one of these square pulses would provide the trigger signal for a sampled point on a subsequent square pulse. The difference in time between the trigger signal and the sampled point would be increased in a fixed manner for later sampled points. All of these sampled points are stored in memory and displayed on the oscilloscope as a series of dots, which corresponds to the waveform. The problem with this triggering scheme is the actual variation in the separation between square pulses. A laser pulse is fired every time the absorption dye is bleached, but this does not occur at intervals of 0.1 seconds exactly. So then the electrical square pulses are not separated by

exactly 0.1 seconds either. Since the sampling measurement is made of a signal which is less than 100 picoseconds duration, the time variation between square pulses is sufficient to randomize the triggering. The time interval between the trigger signal and the sampled point cannot be increased in a fixed way. The solution lies in using the laser pulse itself for the trigger signal. The light pulse is allowed to pass through a beam splitter (figure 4.4, insert). One portion goes to a photodetector which is connected to the trigger of the sampling scope. The other portion is reflected back and forth between prism mirrors in a time delay manner (75nS or greater), before the light pulse falls on the LASS. Subsequently, an electrical square pulse travels to the sampling scope input.

In as much as there is an impedance mismatch between the microstrip line (characteristic impedance of ~100mΩ) and the SMA coaxial cable (characteristic impedance of 50Ω), chip resistors (Dale) are soldered onto the end of the microstrip line to minimize reflections and allow the square pulse to pass onto the SMA coaxial cable with minimal distortion. The chip resistors in parallel make up a very low resistance which terminates the microstrip line. This low resistance, which has a value close to the microstrip line characteristic impedance, is itself in parallel with 50Ω which represents the SMA coaxial cable. Thus, in essence, the square pulse will see the low resistance for an approximate impedance match.

An Nd-YAG laser manufactured by Quantel sends out pulses of light with a center wavelength of 1.06μm to close the switch

(LASS). A Scientech 362 Laser Power Meter including a calorimeter for the detector measures the average energy of a pulse to be 20mJ. The repetition rate of the pulse train is 10Hz and the pulse duration is 30ps. For the LASS experiments high intensity fast rising pulses of light are necessary to activate the LASS. These pulses are generated by the Nd-YAG laser through mode-locking and Q-switching. A schematic of the laser is shown in figure 4.5. Mode-locking causes the oscillation modes within a laser cavity to have a fixed phase relationship with each other. These oscillation modes will then frequency beat with one another to produce short pulses. Mode-locking may be acheived by placing an acousto-optic modulator within a laser cavity. The acousto-optic modulator acts as a window which opens and closes periodically. Single mode oscillation and multimode oscillation cannot exist in such a laser cavity. When the acousto-optic modulator is in its closed cycle high energy losses occur, preventing any oscillation from building up. However, a mode-locked pulse can exist in this laser cavity if the pulse passes through the acousto-optic modulator precisely when it is open. The time period between successive openings of the acouto-optic modulator must be the same as the time between pulses in the pulse train. This is the amount of time necessary for light to transverse the laser cavity length twice.

Mode-locking may also be acheived through placing a saturable dye absorber within the laser cavity somewhere along the optical path. The saturable dye absorber becomes less and less opaque as the optical intensity increases. Since a mode-locked pulse will have higher peak intensities (coherent sum) than a

FIGURE 4.5 Nd-YAG laser schematic

1 Dye Circulation Package
2 Flowing Dye Cell
3 Acousto Mode-Locker
4 Pinhole
5 Dielectric Polarizer
6 Nd-YAG Lasing Medium
7 Translation Stage
8 Diverging Lens
9 Converging Lens
10 Pulse Slicer
11 Turning Mirror
12 Laser Amplifier
13 Quarterwave Plate
14 Isolator
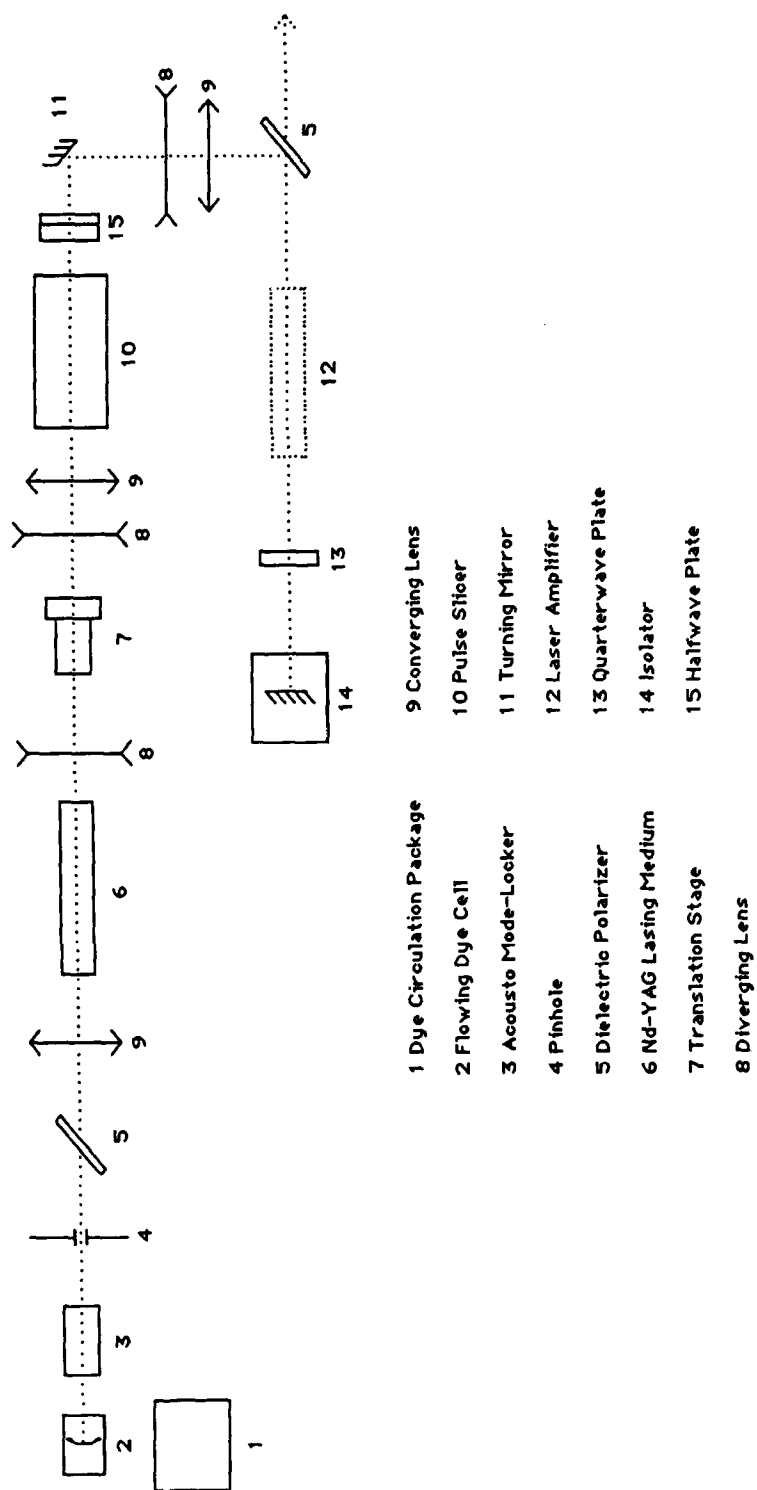15 Halfwave Plate

multimode oscillation with random phase, the existence of a mode-locked pulse will be favored in such a laser cavity [2].

Both an acousto-optic modulator and a saturable dye are used in the Nd-YAG laser for mode-locking. Using a saturable dye alone would require a high dye concentration to stabilize the output energy and to eliminate misshots, this would result in pulses with peak intensities sufficient to damage the optical components. A saturable dye absorber with a low dye concentration may be used with an acousto-optic modulator to secure the same advantages without the possibility of damage to the optical components.

Q-switching enables high intensity light pulses to be produced. The quality factor of a laser cavity is lowered so that the population inversion, and thus the gain, may be increased to a high value. The quality factor then becomes its high normal value as the maximum inversion is approached. The laser oscillation which follows builds quickly to a high intensity, generating the light pulse. Q-switching in the Nd-YAG laser is acheived through the use of the saturable dye. In the beginning, the light passing through the cavity will have a low intensity so the saturable dye will be very opaque and dissipate the energy: Increased power dissipation in the laser cavity means a reduction of Q. Later on, the light will have a higher intensity which results in the saturable dye becoming less opaque and a reduction in the energy loss: Decreased power dissipation in the laser cavity implies an increased Q. Thus, the Q will change from a low value to a high value. Q-switching enables a high power light pulse to be produced, so that a fast-rising electrical pulse may be generated [2]. As discussed

previously in section 3-2 a short risetime is possible for any particular current density if the corresponding carrier density is generated in a short enough time. This requires light energy to be delivered in a short interval, implying high power. Q-switching is then the means by which high power is acheived. In the next chapter, we will see that the laser power is sufficient to generate an electrical pulse with a subnanosecond risetime.

4.5 DISCUSSION

LASS devices with a breakdown voltage of 1kV at microamperes leakage current, have been fabricated through the procedures described in section 4.1. Whether these procedures are sufficient to enable us to reach the limits of the breakdown voltage imposed by the manufacturing process remains to be seen. The placement of the LASS onto the transmission line according to the arrangement in section 4.3 results in a small enough impedance mismatch that a subnanosecond risetime pulse can be measured (see section 5.3). Of course the laser pulse power is consequently great enough to bring about this result. However, the laser pulse power impinging on the LASS is reduced by the passage back and forth among the mirrors because the light spreads out. For future experiments where greater power is necessary, an area of exploration might be to use optical fibers to guide the light.

Sampling measurements with the novel triggering scheme has proven itself to be workable because successive electrical pulses are sufficiently identical. There had been concerns that variations in the laser pulse might cause these electrical pulses to

be different enough with respect to one another so as to preclude the use of sampling techniques. However, this is not the case since each laser pulse has more than the necessary energy to close the switch completely. Otherwise we would need to resort to the more expensive way to measure picosecond signals with a multi-gigahertz digitizer. This would allow measurements to be made in real time of one electrical pulse instead of the need to use information from many pulses as in sampling measurements. We note also that misshots in the laser do not affect our sampling measurements, because the sampling is taken only when triggered by a laser pulse. The measurement techniques and apparatus described in the previous section have been implemented to obtain the results in the next chapter.

References:

1. Davies, R., F. Gentry, "Control of Electric Field at the Surface of P-N Junctions," IEEE Transactions on Electron Devices, vol.ED-11 , pp.313-323, 1964.

2. Yariv, A., Optical Electronics. New York: Holt, Rinehart and Winston, 1985, Ch.6.

CHAPTER 5: LASS EXPERIMENTAL RESULTS

5.0 INTRODUCTION

When the LASS-Microstrip Assembly is placed into the measurement scheme as described in the previous chapter, various experiments may be performed. In the next section we describe some square pulse waveforms generated from the LASS. In succeeding sections we describe the measurement of the current density and the risetime of the pulse.

5.1 OBSERVATION OF THE WAVEFORM

To observe the square pulse waveform on the oscilloscope the transmission line (left side) is charged up to several hundred volts and a laser pulse closes the LASS. Ideally the pulse shape would be the same as that shown in figure 5.1. However, the oscilloscope trace which is reproduced photographically in figure 5.2(a), shows distortions to this ideal case. We note that at point "a" (figure 5.2(a)), which precedes the leading edge of the square pulse, there are various voltage peaks. The distortion here is due to laser prepulse. In practice, the laser pulse does not rise up suddenly from zero energy; some energy is emitted before the main body of the pulse. This energy generates some carriers in the LASS, which allows some current to pass through. Thus, the distortion at point "a" is the result. Neutral density filters lower the overall energy of the laser pulse so that most of the prepulse is eliminated. The main body of the pulse continues to have more than enough energy to close the LASS after passing through the filters.
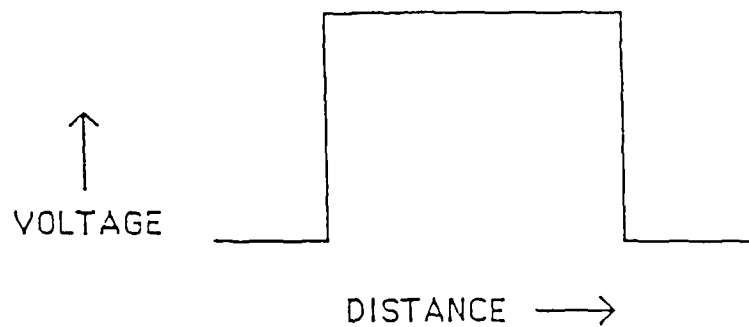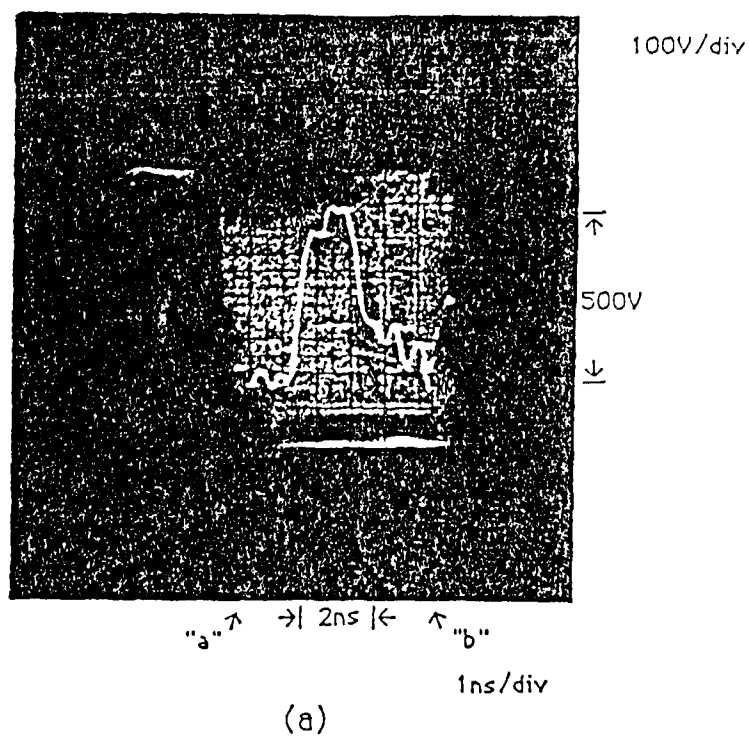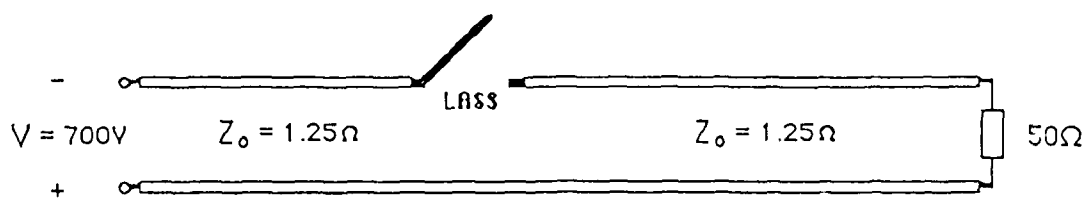
45

VOLTAGE

DISTANCE ⟶

FIGURE 5.1 Ideal pulse waveform

(a)

(b)

FIGURE 5.2 Current density measurement: (a) oscilloscope trace in real time, (b) circuit schematic.

In addition, the back edge of the square pulse (point "b", figure 5.2(a)) shows heavy distortion. As discussed in the previous chapter (section 4.3), this is due to the positioning of the charging wires at the trailing edge of the transmission line. Consequently a discharge of these wires adds a distortion to the trailing edge of the pulse. Much of this distortion is removed by attaching the wires near the center of the conductor. Then the square pulse waveform is much closer to the ideal case when these two changes are made (figure 5.3(a)).

5.2 CURRENT DENSITY

From figure 5.2(a) the current density may be obtained since the concern here is the height of the pulse and not its leading or trailing edge. Figure 5.2(b) is a schematic of the circuit in this experiment and the Tektronix 7834 (without sampling) is used. The transmission line is fabricated by a vendor, has a characteristic impedance of 1.25Ω, and is not terminated with this resistance. Therefore, in as much as the transmission line is joined to a coaxial cable with an impedance of 50Ω, the voltage height will double at this point. Since the charging voltage is 700V, the square pulse will have a voltage of 350V moving down the transmission line and will double in voltage at the end. The expected measured voltage will then be 700V. From figure 5.2(a) a value of 500V is obtained. The 200V difference can be attributed to voltage drops across the diode and along the transmission line. Also the transmission factor is not exactly 2, in going from the

transmission line to the SMA cable ((2x50)/(1.25+50)=1.95; 1.95x350=683V). An approximate value for the current density may be obtained from equation (3-1), knowing that the diode dimensions are 1mm by 2mm:

$$J = \frac{V/2}{Z_o}\left(\frac{1}{Wd}\right) = \frac{(500V/2)}{(125\Omega)(0.1cm)(0.2cm)} = 10\frac{kA}{cm^2} \quad (5\text{-}1)$$

The assumption here is the pulse height passing through the LASS is 250V (500V/2). However, this is the value measured at the oscilloscope. Since there is a voltage drop along the transmission line, from the LASS to the oscilloscope, the actual pulse height at the LASS would be a value greater than 250V.

If we assume the entire 20mJ laser pulse is absorbed and generates carriers, the carrier density can be estimated. Assuming unity quantum efficiency, the number of carriers N is approximately,

$$N = \frac{20x10^{-3}J}{1eV} = \frac{20x10^{-3}J}{1.6x10^{-19}J} = 1.25x10^{17} \quad (5\text{-}2)$$

If the thickness of the diode is 0.08cm, then the carrier density is

$$n = \frac{N}{volume} = \frac{1.25x10^{17}}{(0.08cm)(0.1cm)(0.2cm)} = 7.81x10^{19}cm^{-3} \quad (5\text{-}3)$$

However, if we consider the number of states available into which an electron may be photoexcited in the conduction band by a 1.06μm wavelength laser light, this carrier density is too large. The number of states per unit volume N_s from the conduction band edge E_c to an arbitrary energy level E, may be calculated in the following way:

$$N_s = \int_{E_c}^{E} N(E')dE = \frac{(2m)^{3/2}}{2h^3\pi^2} \int_{E_c}^{E} (E - E_c)^{1/2} dE = \frac{6.81 \times 10^{21}}{eV^{3/2}cm^3} (2/3)(E - E_c)^{3/2} \quad (5\text{-}4)$$

where N(E) is the density of states [1]. As the energy level E becomes further removed from the conduction band edge, the excitation to these higher energy levels becomes more improbable. After all, the great majority of photons will have an energy close to the value which is necessary to excite an electron from the valence band edge to the conduction band edge. Calculating N_s for values of ($E-E_c$) using the above equation,

($E-E_c$)	N_s
1kT (0.025eV)	1.79×10^{19} cm^{-3}
2kT (0.050eV)	5.08×10^{19} cm^{-3}
3kT (0.075eV)	9.32×10^{19} cm^{-3}

where T is the room temperature. In order for the entire laser pulse to be absorbed, generating 7.81×10^{19} carriers/cm^3, electrons must be excited up to an energy level which is almost 3kT above E_c. This is highly unlikely, given the energy necessary for such an excitation. If all of the states up to 1kT are used, which is assumed to be reasonable, only a small fraction of the laser pulse energy will create carriers. The rest of the energy is wasted. Of course, all of the energy could be absorbed if the volume of the device is sufficiently large, but the ratio of the carriers to the volume (carrier density) would remain the same so this does not help us in acheiving a higher current density.

We note that before photon irradiation many of the states near the conduction band edge are already occupied according to the

Fermi-Dirac statistics, which give the probability of occupancy in an energy state. Of course this decreases the number of carriers that can be generated, since the number of states into which an electron can move is reduced. Also, we assumed in the above that electrons are only excited from the valence band edge. In reality, after all the electrons are excited from those states at the valence band edge, excitation must occur from lower energy states within the valence band. This requires an additional energy for across bandgap excitation. Since this lowers the maximum energy level to which an electron can be excited, this further reduces the number of states into which an electron can move in the conduction band.

Assuming when electrons are excited into the conduction band all of the states up to 1kT are available and assuming a typical value for the drift velocity, we can apply equation 3-2 and obtain an estimate of the maximum current density possible:

$$J = nev_d = (1.79 \times 10^{19} cm^{-3})(1.6 \times 10^{-19} c)(2 \times 10^6 \frac{cm}{s}) = 5.73 \frac{MA}{cm^2} \quad (5-5)$$

Thus, when comparing this value with the $10kA/cm^2$ from experiment we understand that only a small fraction of the carriers generated are being used.

From equation (3-3) we obtain the switch power density where V is the voltage in the "open" state:

$$P = V \times J = (700V)(10 \frac{kA}{cm^2}) = 7 \frac{MW}{cm^2} \quad (5-6)$$

If we then multiply this by the area A

$$P \times A = (7 \frac{MW}{cm^2})(0.1cm)(0.2cm) = 0.14 MW \quad (5-7)$$

This value for the power falls far short of the ten megawatts demonstrated at Lawrence Livermore National Laboratory, but does indicate the power handling capacity of the LASS [3]. To obtain a value for the gain G we must first find the approximate energy of the pulse $W_{\mu w}$. Using the form of the above two equations to find the average power P_{avg} by replacing 700V with the pulse height 250V,

$$P = (250V)(10\ \frac{kA}{cm^2}) = 2.5\ \frac{MW}{cm^2} \quad (5\text{-}8)$$

$$P_{avg} = P \times A = (2.5\frac{MW}{cm^2})(0.1cm)(0.2cm) = 0.05\ MW \quad (5\text{-}9)$$

Then from figure 5.2(a) the pulse length is estimated to be 2ns so that

$$W_{\mu w} = P_{avg} \times l_p = (50\times10^3 W)(2\times10^{-9}s) = 0.1\ mJ \quad (5\text{-}10)$$

From the previous chapter W_{ph} has a measured value of 20mJ. Applying equation (3-5)

$$G = \frac{W_{\mu w}}{W_{ph}} = \frac{(0.1mJ)}{(20mJ)} = 5\times10^{-3} \quad (5\text{-}11)$$

This value for the gain is obviously many magnitudes smaller than what is desired. This is not surprising, because of the value in the denominator. As noted in the above discussion only a small fraction of the 20mJ will generate carriers, and of the carriers generated by this energy, only a small portion will participate in the current flow. Therefore, although 20mJ is the optical input energy, much of it is not involved in the production of the output pulse. Then the output pulse energy is being compared to an input

energy which is too large. A more reasonable value for the gain would be obtained if only the fraction of the input energy involved in the pulse generation process is used. The carrier density which would allow 10 kA/cm^2 to flow is

$$n = \frac{10\frac{kA}{cm^2}}{(1.6 \times 10^{-19} c)(2 \times 10^{6}\frac{cm}{s})} = 3.13 \times 10^{16} cm^{-3} \quad (5\text{-}12)$$

From a previous calculation 20mJ would generate $7.81 \times 10^{19} cm^{-3}$ if all of that energy could be absorbed, so then the energy E which is necessary to create the carrier density n is

$$E = (3.13 \times 10^{16} cm^{-3})\frac{(20mJ)}{(7.81 \times 10^{19} cm^{-3})} = 8 \times 10^{-3} mJ \quad (5\text{-}13)$$

Then using this value for the optical input energy in the equation for gain,

$$G = \frac{(0.1mJ)}{(8 \times 10^{-3} mJ)} = 12.5 \quad (5\text{-}14)$$

Obviously, this gain is much closer to expectations. As higher power levels are explored we anticipate larger values for the gain.

5.3 RISETIME MEASUREMENT

In figure 5.3(a) the square pulse risetime is measured through the use of the sampling unit. Figure 5.3(b) shows the circuit schematically. The length L for a pulse of 1.1ns can be calculated:

$$L = \frac{(1.1ft)}{\sqrt{\varepsilon}} = \frac{(1.1ft)}{\sqrt{2.6}} = 0.68 ft = 8.16 in. \quad (5\text{-}15)$$

This is close to the actual pulse length of 6 inches as determined

100mV/div

REDUCED SCAN
(Small Squares)

→| 1.1ns |←
→| |← 200ps

200ps/div

(a)

V = 1V $Z_0 = 2.95\Omega$ LASS $Z_0 = 2.95\Omega$ 3.89Ω   50Ω
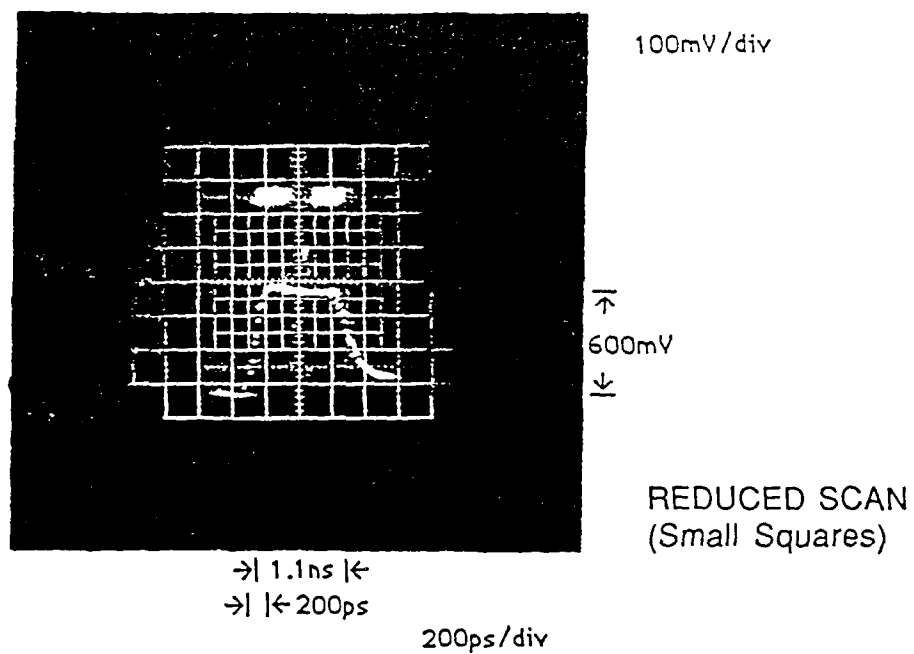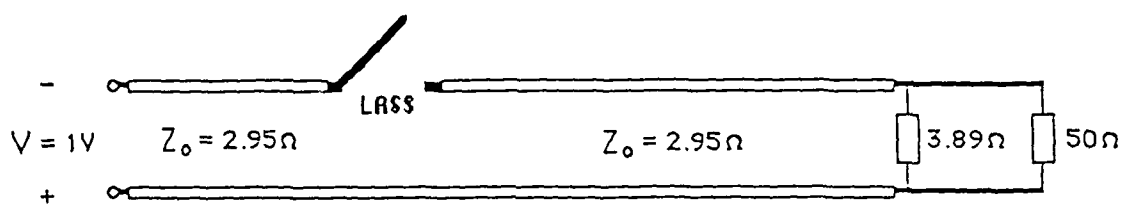
(b)

FIGURE 5.3 Risetime measurement: (a) oscilloscope trace with sampling, (b) circuit schematic.

by measuring the transmission line on the left side (figure 5.3(b)) as being 3 inches and then doubling it. The 1.1ns is measured from the front to the back of the pulse at the point halfway up to the height. In as much as the length may be measured between two different points (ie. 0.63 x height), the arbitrary nature of this choice could account for the discrepancy in the pulse lengths.

The characteristic impedance is calculated from equation (3-7). The thickness h of the dielectric is 10 mils. or 0.0254 cm.

$$Z_o = \frac{120\pi}{\sqrt{\varepsilon}} \frac{h}{W} = \frac{120\pi}{\sqrt{2.6}} \frac{(0.0254cm)}{(2cm)} = 2.95 \ \Omega \quad (5\text{-}16)$$

This 2.95Ω transmission line is terminated with a resistance of 3.89Ω. The 50Ω of the SMA cable attached to the end of the transmission line, is in parallel with the 3.89Ω termination so that in essence there is 3.89Ω at the end of the transmission line. The transmission coefficient is 1.1 (2x3.89/(2.95+3.89)). The transmission line is charged to 1V. Then the square pulse should have a voltage height of 500mV when traveling down the line and after passing onto the SMA cable the voltage should be 550mV (500x1.1). 600mV is measured in figure 5.3(a) which corresponds fairly well with 550mV.

From figure 5.3(a) the approximate risetime of the square pulse is 200ps. This value is far greater than the 1ps risetime we hope to measure in the future, which is possible according to theory. In fact Bell Laboratories has demonstrated a 25ps risetime [2]. The laser pulse in our experiments has an energy of 20mJ and a pulsewidth of 30ps. A subject for future investigation is whether

or not there is enough energy delivered in 1ps to close the switch. If this is not the case, the laser system that is presently being used would be inadequate to demonstrate a 1ps risetime at any current density. Also the risetime degradation due to the impedance mismatch must be sufficiently resolved.

5.4 CONCLUSION

Experiments involving pulse generation with the LASS-microstrip assembly has resulted in several accomplishments. A square pulse waveform which is close to the expected shape has been observed after suppressing the laser prepulse and altering the transmission line charging method. A value of 10kA/cm^2 for the current density has been obtained with the understanding that only some of the carriers generated are participating. An indication of the power handling capacity of the LASS can be seen in the value for the power of 0.14MW. A modest gain of 12.5 is estimated which is the ratio between the output electrical energy and the input optical energy. A 200ps risetime is measured through a sampling technique. Improvements in technical expertise will lead to better values for these parameters. We have attempted to measure high current density and fast risetime separately, because this is easier from a technical standpoint. Of course, to demonstrate simultaneously both high current density and fast risetime is a goal of future research.

References:

1. Warner, R., B. Grung, Transistors. New York: Wiley, 1983, Ch.2.

2. LeFur, P., D. Auston, "A Kilovolt Picosecond Optoelectronic Switch and Pockel's Cell," Applied Physics Letters. vol.28, p.21, 1976.

3. Zucker, O., J. Long, V. Smith, D. Page, P. Hower, "Experimental Demonstration of High-Power Fast-Rise-time Switching in Silicon Junction Semiconductors," Applied Physics Letters. vol.29, pp.261-263, 1976.

CHAPTER 6: CONCLUSION AND PERSPECTIVE

Presently, the LASS-microstrip assembly generates electrical pulses which result in a current density of $10kA/cm^2$ and a risetime of 200ps. These values illustrate the potential of the LASS and microstrip line to generate pulses of high current density and fast risetimes.

As the impedance mismatch between the diode and transmission line is reduced by improving the connection there (see discussion below), faster risetimes will be measured. In addition the power of the laser may be investigated to see what is the shortest time possible for closing the switch, when the impedance mismatch is minimized.

To set up a measurement, various connections must be made: Between the charging cables and the transmission line, the LASS and the transmission line, and the transmission line and the coaxial cable. These connections must be made better, because they affect to a significant degree the electrical pulse that is generated. We noted in section 5.2 how moving the connection between the charging cables and the transmission line leads to an improvement in the pulse waveform. To improve the impedance mismatch between the LASS and the transmission line, the connection over there must be modified in some way, which is an area for future exploration. In section 4.3 we have described how the LASS is electrically joined onto the transmission line through copper strips. One end of the copper strip is applied with mechanical pressure to the LASS. This is not a good coupling. Hot soldering is unacceptable because the heat might damage the LASS. Different

57

possibilities have been tried such as cold solder and silver paint, but to no effect. Also something other than a copper strip might be used to enhance the connection. The connection between the transmission line and the coaxial cable needs to be studied to reduce any adverse effects due to impedance mismatch such as degradation of the waveform and energy loss. Chip resistors have been used to terminate the line in an attempt to obtain a better impedance match. However, there has been difficulty moving in this direction in as much as the available chip resistors have resistance values, larger than desired to create the necessary resistance by placing several of them in parallel.

As the breakdown voltage of the diode is increased and the characteristic impedance of the transmission line is reduced, we anticipate a much higher current density. The fabrication of low impedance transmission lines forms an interesting technical problem. There are vendors which provide copper-cladded dielectrics useful for fabricating high impedance lines, but none with dielectric thicknesses enabling the creation of a line with a characteristic impedance below 0.1Ω. Therefore, it is necessary to take a very thin dielectric material and try to metallize both sides either through evaporation, deposition, or electroplating. The difficulty here is that these methods are imperfect.

Laser light coupling through the side surface passivation is acceptable in as much as the passivation layer seems sufficiently transparent to allow enough light to enter to close the switch. An investigation can be made of the passivation layer to discover the

degree it is transparent to infrared light. Also we need to know if the passivation layer can be improved to avoid its deterioration with time. These issues must be resolved on the experimental side.

On the theoretical side, maximization of the current density and the effect of impedance mismatch and laser power on the risetime, can be explored through a deeper understanding of the carrier generation, charge transport phenomena in high electric field region in silicon. Whether this will lead to agreement with experimental results remains to be seen.

An issue which will be dealt with later is how to maximize the absorption efficiency. Theoretically attempts can be made to better establish the relationship of absorption efficiency to the material doping and the number of carriers. Experimentally this relationship can be clarified if the number of carriers can be ascertained. Since the current density can be measured, the product of the drift velocity and carrier concentration is known. The carrier concentration can then be determined if an independent means is found to obtain the drift velocity. One possibility might be to use a modification of the Time of Flight measurement technique [1]. The absorption efficiency can then be optimized with its relationship to the number of carriers and the material doping well understood.

Once the various technical problems are resolved, energy compression with the LASS-microstrip assembly will provide a source of high-power fast risetime pulses. Wherever such pulses are needed in various applications, this device can be an alternative, and possibly an improvement, to whatever previous

source had been used. In addition this device will open up new areas of application because of its unique characteristics (high power with high switching speed). Several of these sources may be placed together in parallel, in series, or a combination of both to generate pulse trains. Pulse trains of different patterns can be easily realized, because picosecond timing of each source with respect to one another is no problem. All that is needed is to vary the length of optical fibers that deliver the laser pulse to each source. As we mentioned previously in section 2.2, an array of such sources which are properly timed can produce a microwave burst, but now at high power levels. So in closing, generation of high-power fast risetime pulses with the LASS has a very promising future.

References:

1. Reggiani, L., <u>Hot-Electron Transport in Semiconductors.</u> New York: Springer-Verlag, 1985, Ch.3.

```fortran
c This program use reference direction as v0-->[n-i-p]-->load
c                                           ----------->x
        program lass
        implicit real *8 (a-h,p-z)
        real *8 nd,h,nn,np,na,nii,jnd,jpd,et,id,an(121),ap(121),g(121)
        real *8 n(121),p(121),n1(121),p1(121),n0(121)
        real *8 ,p0(121),un(121),up(121),gan(121),gap(121)
        real *8 dn(121),ni(121),dp(121),e(121),e1(121),k
        real *8 e2(121),jn,jp,jd,jt,jta,us
        character otfile*10,dat*10,type*10
        integer i,l,nl
        common /e/ t0,sd,q0,k,e0,q,n,p
        common /d/ nll,hh,ii
c
        print *,'enter dat.file'
        read *,dat
        open (unit=10,file=dat,status='old')
 21     print *,'file name'
        read (10,*,end=1011) otfile
        open (unit=9,file=otfile,status='new')

c the dielectric and magnetic permittvity for the diode is 'es' and 'us'
        e0=8.85418d-14*11.9
        us=1.255492781d-8
c impedance 'z0'  of the stripe
c 'nl' # of subzones for the one dimensional diode
        nl=121
        nll=nl-2
c 'q' : unit charge volumn
c 'e0' : dielectric permitivity of the silicon
c 'td' : device temperature
c 'k' : boltzmann constant
c 'uni' : mobility of electrons
c 'upi' : mobility of holes
c 'ece,ech' : critical electric field of electron and hole
c 't0' : time when peak of the incident light is reached
c 'sd' : deviation of the gaussian curve
c 'an,ap' :impact ionization coefficeint of electron and hole
c 'gan,gap' :electron and hole generation due to impact inoization
        q=1.6d-19
        td=300.
        k=1.38066d-23
        uni=1350
        upi=480
        ece=8.d3
        ech=2.d4
        print *,'enter "t0"'
        read (10,*) t0
        print *,'enter "FWHM" of laser pulse'
        read (10,*) fwhm
        sd=fwhm/2./sqrt(log(2.))
        print *,'Enter simulation data:'
        print *,'----------------------'
c 'q0' : input light intensity
c 'gt' : # of electron and hole pairs generated for each step
c 'error' : error in each step
        print *,'input q0='
        read (10,*) q0
        print *,'input gt='
        read (10,*) gt
        print *,'input error='
        read (10,*) error
        print *,'enter final time "tf"'
        read (10,*) tf
        print *,'enter z0'
        read (10,*) z0
```

```fortran
      r=z0
c 'h' :delta x
c 'w' :width of the intrinsic region
c 'a' :surface area of the planar diode
c 'va' :applied biasing voltage
      print *,'enter width = ?'
      read (10,*) w
      h=w/(nl-1)
      print *,'enter "a"'
      read (10,*) a
      print *,'enter applied voltage'
      read (10,*) va
      print *,'q0=',q0
      print *,'gt=',gt
      print *,'error=',error
      print *,'z0= ',z0

c-------------------------------------------------------------------
c this loop is used to calculate the total amount of electron-hole-
pairs concentration generated within 400ps
      do 300 i=1,4000
        t=i*1.d-13
        gl=q0*exp(-(t-t0)*(t-t0)*1.d24/sd/sd)
        gtol=gtol+gl
 300    continue
      gnp=gtol*1.d-13
      print 1040,gnp,w
 1040   format ('g.of.np=',e9.3,3x,'pnwidth=',e9.3)
c initial condition for depletion region:
c 'nd', 'ni' and 'na' are the backing doping concentrations for the
c n-region, i-region and p-region respectively
c n=p=0 when time at zero
      print *,'enter nd'
      read (10,*) nd
      print *,'enter na'
      read (10,*) na
      print *,'enter ni'
      read (10,*) nii
c For different biasing voltage, the intrinsic region can be either
fully depleted or partially depleted.
c I. for completely depleted intrinsic region:
      if (va .ge. q/2/e0*(nii+nii*nii/na)*w*w) then
      aa=nd+nd*nd/na
      b=2*(nd+2*nd*nii/na)*w
      c=-2*e0*va/q+(nii+nii*nii/na)*w*w
      xn=(-b+sqrt(b*b-4*aa*c))/2/aa
      xp=nd/na*xn+nii/na*w
      nn=xn*nd
      np=xp*na
      print *,'P-I-N'
c equivalent surface charge in the n-i boundary
      print *,'nn=',xn*nd
c equivalent surface charge in the i-p boundary
      print *,'np=',xp*na
c 'xn' :n-depletion region width
      print *,'xn=',xn
c 'xp' :p-depletion region width
      print *,'xp=',xp
      print *,xn,' ',q*nd*xn/e0
      print *,w+xn,' ',q*na*xp/e0
      print *,w+xn+xp,' 0'
c    initial value
      enn=nn*q/e0
      enp=np*q/e0
```

```fortran
            e(i)=((epp-enn)*(i-1))/(nl-1)+enn
            ni(i)=nii
10       continue
         et=0.
         do 30 i=1,nl
         print *,e(i)
            n(i)=0.
            p(i)=0.
            n0(i)=0.
            p0(i)=0.
         gan(i)=0.
         gap(i)=0.
         g(i)=0.
            el(i)=e(i)
            et=et+e(i)
            x=e(i)/ece
            x=1+x*x
            x=sqrt(x)
            un(i)=uni/x
            x=1+e(i)/ech
            up(i)=upi/x
            dn(i)=k*td*un(i)/q
            dp(i)=k*td*up(i)/q
30       continue
         v0=(et-enn/2-epp/2)*h
         print *,'v0= ',v0
         print *,'===================='
         print *,' '
c II. for the partially depleted intrinsic region
         else
         type='pn'
         w1=sqrt(2*e0*va/q/(nii/na+nii))
         xp=w1*nii/na
         np=xp*na
         print *,'P-I'
         print *,'np=',xp*na
         print *,'xn=',w1
         print *,xp,' ',q*na*xp/e0
         print *,w1+xp,' 0'
c    initial value
         np=xp*na
         epp=np*q/e0
         enn=0.
         do 12 i=1,nl
            if ( (nl-i)*h .ge. w1 ) then
            e(i)=0.
            ni(i)=nii
            else
            e(i)=(1-(nl-i)*h/w1)*epp
            ni(i)=nii
            end if
12       continue
         et=0.
         do 31 i=1,nl
         print *,e(i)
            n(i)=0.
            p(i)=0.
            n0(i)=0.
            p0(i)=0.
         gan(i)=0.
         gap(i)=0.
         g(i)=0.
            el(i)=e(i)
            et=et+e(i)
            x=e(i)/ece
```

```
              x=sqrt(x)
              un(i)=uni/x
              x=1+e(i)/ech
              up(i)=upi/x
              dn(i)=k*td*un(i)/q
              dp(i)=k*td*up(i)/q
 31        continue
           xn=1d-8
           v0=(et-enn/2-epp/2)*h
           print *,'v0= ',v0
           print *,'=================='
           print *,' '
           end if


c------------------------------------------------------------
c  Main Program
           t=0.
           va=v0
           id=0
           count=0.e-12
           nc=0

 5         if (t .gt. tf) go to 3
c 'time' subroutine is used to determine the 'dt' for a given
c generation 'g'
           call time(t,dt,g,gt,nnn)
 9         do 302 i=1,nl
              n(i)=n0(i)
              p(i)=p0(i)
              e(i)=el(i)
 302       continue
           nc=nc+1
c calculate n and p bye the 'continuity equation'
 1         do 14 i=2,nl-1
           p1(i)=(dp(i)*(p(i+1)+p(i-1))*dt/h/h+(g(i)+gan(i)+gap(i))*dt+
     *            p0(i)-d1(1,dp,i)*p(i-1)/h*dt+up(i-1)*e(i-1)*p(i-1)/h*dt)/
     *            (1+2*dp(i)*dt/h/h+
     *            up(i)*e(i)/h*dt-d1(1,dp,i)/h*dt)

           n1(i)=(dn(i)*(n(i+1)+n(i-1))*dt/h/h+(g(i)+gan(i)+gap(i))*dt+
     *            n0(i)+d1(2,dn,i)*n(i+1)/h*dt+un(i+1)*e(i+1)*n(i+1)/h*dt)/
     *            (1+2*dn(i)*dt/h/h+
     *            un(i)*e(i)/h*dt+d1(2,dn,i)/h*dt)
 14        continue
c boundary condition
           p1(1)=((g(1)+gan(1)+gap(1))*dt+p0(1))/
     *            (1+up(1)*e(1)/xn*dt)
           n1(1)=((g(1)+gan(1)+gap(1))*dt+n0(1)
     *            +d1(2,dn,1)*n(2)/h*dt+un(2)*e(2)*n(2)/h*dt)/
     *            (1+un(1)*e(1)/h*dt+d1(2,dn,1)/h*dt)
           p1(nl)=((g(nl)+gan(nl)+gap(nl))*dt+p0(nl)
     *            +(-d1(1,dp,nl)+up(nl-1)*e(nl-1))*p(nl-1)/h*dt)/
     *            (1+up(nl)*e(nl)/h*dt-d1(1,dp,nl)/h*dt)
           n1(nl)=((g(nl)+gan(nl)+gap(nl))*
     *            dt+n0(nl))/(1+un(nl)*e(nl)/xp*dt)
c check convergence of n,p with n1,p1
           check=0.
           total=0.
           do 7 i=1,nl
              en=n(i)-n1(i)
              ep=p(i)-p1(i)
              check=max(check,abs(en/n1(i)))
              check=max(check,abs(ep/p1(i)))
              p(i)=p1(i)
              n(i)=n1(i)
```

```fortran
            total=total+(p(i)-n(i))*h
7           continue
            total=total-(p(nl)+p(1)-n(nl)-n(1))/2*h
            total=total+(p(1)-n(1))*xn+(p(nl)-n(nl))*xp
c calculate the corresponding electric field for a given n and p.
c electric field were calculated by the Maxwell equation
111         check1=0.
            do 60 i=1,nl
              et=0.
              va=v0-(e(nl)+e(1))*h/2
              do 70 j=2,nl-1
              et=et+e(j)
70            continue
              if (i .eq. 1) then
              e2(1)=((va-(et-e(1))*h)/2./a/r
     *            +e0*e1(1)/dt)/
     *            (q*(un(1)*n(1)+up(1)*p(1))+e0/dt+h/2./a/r)
              else if (i .eq. nl) then
              e2(nl)=((va-(et-e(nl))*h)/2./a/r
     *            +e0*e1(nl)/dt)/
     *            (q*(un(nl)*n(nl)+up(nl)*p(nl))+e0/dt+h/2./a/r)
              else
              e2(i)=((va-(et-e(i))*h)/2./a/r-q*(dn(i)*dl(2,n,i)-
     *            dp(i)*dl(1,p,i))+e0*e1(i)/dt)/
     *            (q*(un(i)*n(i)+up(i)*p(i))+e0/dt+h/2./a/r)
              end if
              ee=e(i)-e2(i)
              check1=max(check1,abs(ee/e2(i)))
              e(i)=e2(i)
60          continue
            if (check1 .gt. 1d-13) go to 111

c check the convergence of the electric field.
            et=0.
            do 100 i=2,nl-1
            et=et+e2(i)
              ee=e(i)-e2(i)
              check=max(check,abs(ee/e2(i)))
100           continue
            sign=v0-(et+e(1)/2+e(nl)/2)*h
            do 120 i=1,nl
              x=e(i)/ece
              x=1+x*x
              x=sqrt(x)
              un(i)=uni/x
              x=1+e(i)/ech
              up(i)=upi/x
              dn(i)=k*td*un(i)/q
              dp(i)=k*td*up(i)/q
            an(i)=e(i)/3.6*exp(-1.954d6/(e(i)*(1+e(i)/1.069d5)+1.357d4))
            ap(i)=e(i)/5.0*exp(-3.091d6/(e(i)*(1+e(i)/1.11d5)+1.545d4))
120           continue
            do 133 i=2,nl-1
            gan(i)=an(i)*(+dn(i)*dl(2,n,i)+un(i)*e(i)*n(i))
            gap(i)=ap(i)*(-dp(i)*dl(1,p,i)+up(i)*e(i)*p(i))
133         continue
            gan(1)=an(1)*un(1)*e(1)*n(1)
            gap(1)=ap(1)*up(1)*e(1)*p(1)
            gan(nl)=an(nl)*un(nl)*e(nl)*n(nl)
            gap(nl)=ap(nl)*up(nl)*e(nl)*p(nl)
            print *,'sign',sign
            print *,' '
            if (check .lt. error) go to 2
            go to 1

2           jta=0.
```

```fortran
c 'jn' :electron current
c 'jp' :hole current
c 'jt' :total current
c the current were calculated by the current density equation
          do 191 l=2,nl-1
             jn=q*(dn(l)*dl(2,n,l)+un(l)*e(l)*n(l))
             jp=q*(-dp(l)*dl(1,p,l)+up(l)*e(l)*p(l))
             jd=e0*(e(l)-el(l))/dt
             jnd=q*un(l)*e(l)*n(l)
             jpd=q*up(l)*e(l)*p(l)
             jt=jn+jp+jd
             jta=jt+jta
191       continue
          print *,'total=',total
          id=jta/(nl-2)*a
          print *,'time=',t,'  id=',id
          if (check .lt. error) go to 4
          go to 9
4         do 200 l=1,nl
             n0(l)=n(l)
             p0(l)=p(l)
             el(l)=e(l)
200       continue
          vout=id*z0
          plus=2d-12
          if ( t .ge. count) then
          if (t .gt. 50.e-12) then
          plus=4.e-12
          end if
          if (t .le. 10.e-12) then
          plus=4.e-12
          end if
          count=count+plus
c         print *,' '
          write (9,1111) t,vout
1111      format(2 e12.4)
          do 500 i=1,nl
             write (9,1001) i,e(i),n(i),p(i),an(i),ap(i),gan(i)*dt,gap(i)*dt
1001      format(1x,i3,7 e10.3)
500       continue
          write (9,1002)
1002      format(7x,'rd',8x,'Vout',8x,'Iout',5x,'Power out')
          write (9,1003) va/id-z0,vout,id,id*vout
1003      format(4 e11.4/)
          print *,'time= ',t,'  vout=',vout
          print *,' '
          end if
          go to 5
3         close (9)
          go to 21
1011      close (10)
          end


c---------------------------------------------------------------
          subroutine time(t,dt,g,gt,nnn)
          implicit real *8 (a-h,p-z)
          real *8 k,g(121),n(121),p(121)
          common /e/ t0,sd,q0,k,e0,q,n,p
          common /d/ nl,hh,ii
          dt=0
          dt0=1d-12
          nnn=0
          plus=2d-12
          if (t .ge. 50.e-12) then
          plus=2d-12
          end if
```

```fortran
1         dt=dt+dt0
          nnn=nnn+1
          eg=q0*exp(-(t+dt-t0)*(t+dt-t0)*1.d24/sd/sd)*dt-gt
          if (dt .ge. plus) go to 4
          if (eg .lt. 0.) go to 1
4         t=t+dt
          do 20 i=1,nl+2
c ***** you can do any modification about 'g' here *****
          g(i)=q0*exp(-(t-t0)*(t-t0)*1.d24/sd/sd)
  20      continue
          return
          end


c---------------------------------------------------------------
c 'd1' first order differential operator
          function d1(n,f,i)
          real *8 f(121),h,hh,d1
          integer i,s,n
          common /d/ nl,hh,ii
c
          s=0
          h=hh
          if (n .eq. 1) then
            d1=(f(i)-f(i-1))/h
          else
            d1=(f(i+1)-f(i))/h
          end if
          return
          end


c---------------------------------------------------------------
c 'd2' second order differential operator
          function d2(f,i)
          real *8 f(121),h,d2,hh
          integer i,s
          common /d/ nl,hh,ii
c
          s=0
          h=hh
          if (i .eq. 1) then
            d2=(f(i+2)-2*f(i+1)+f(i))/h/h
          else if (i .eq. nl) then
            d2=(f(i)-2*f(i-1)+f(i-2))/h/h
          else
            d2=(f(i+1)-2*f(i)+f(i-1))/h/h
          end if
          return
          end
```